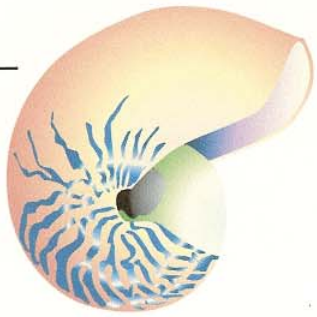

Coastal Marine Institute

University of Alaska

High-Resolution Numerical Modeling of Near-Surface Weather Conditions over Alaska's Cook Inlet and Shelikof Strait

Peter Q. Olsson
Principal Investigator

Co-principal Investigators:
Haibo Liu

Final Report
OCS Study MMS 2007-043

October 2009

Minerals Management Service
Department of the Interior

and the

School of Fisheries & Ocean Sciences

University of Alaska Fairbanks

This study was funded in part by the U.S. Department of the Interior, Minerals Management Service (MMS) through Cooperative Agreement No. M08AR12675, between MMS, Alaska Outer Continental Shelf Region, and the University of Alaska Fairbanks.

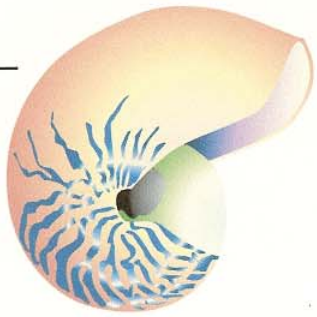

Coastal Marine Institute

University of Alaska

High-Resolution Numerical Modeling of Near-Surface Weather Conditions over Alaska's Cook Inlet and Shelikof Strait

Peter Q. Olsson
Principal Investigator

Co-principal Investigators:
Haibo Liu

Final Report
OCS Study MMS 2007-043

October 2009

Minerals Management Service
Department of the Interior

and the

School of Fisheries & Ocean Sciences

University of Alaska Fairbanks

Contact information

Coastal Marine Institute
School of Fisheries and Ocean Sciences
University of Alaska Fairbanks
P. O. Box 757220
Fairbanks, AK 99775-7220

email: sharice@sfos.uaf.edu
phone: 907.474.7208
fax: 907.474.7204

TABLE OF CONTENTS

LIST OF TABLES

LIST OF FIGURES

ABSTRACT

Along the north Gulf of Alaska coast, terrain plays an important role in determining local weather. High frequency deep synoptic-scale low pressure systems interact with terrain to frequently produce ageostrophic gap and channel winds, often called low-level jets (LLJs) in places like Cook Inlet and Shelikof Strait. These winds may at times be quite strong, with gusts occasionally exceeding 50 ms^{-1}. Understanding and accurately forecasting these winds are critical to mariner and aviator activities in this region. However, due to the paucity of observations, these surface wind regimes are not well documented. Numerical modeling can be used for these purposes.

This work developed an atmospheric modeling capability for Cook Inlet/Shelikof Strait region of Coastal Alaska. A modeling system that is both fast and efficient enough to act as a nowcast/forecast system and versatile enough to be used for a variety of research purposes has been built. This system uses current initialization data that comes to Alaska Experiment Forecast Facility (AEFF), University of Alaska Anchorage via a T1 line from the National Weather Service in Alaska. This system has been used to produce daily weather simulations for the Cook Inlet and Shelikof Strait region. Using this capability, we have systematically studied LLJs and other winds in Cook Inlet and Shelikof Strait.

The comparison between the Regional Atmospheric Modeling System (RAMS) winds and the Synthetic Aperture Radar (SAR)-derived winds when available verifies the existence of these wind jets and the capability of the model to simulate these cases. A climatology of simulated low-level wind jets over the Cook Inlet and Shelikof Strait of Alaska has been composed. The low-level wind jets are classified into 10 different regimes as a function of location and orientation. These regimes are categorized into four more general groups: cross-channel westerly, easterly, and up and down-Inlet flows. The nature of a particular regime is largely a function of pressure gradient orientation and local topography. Jets in the same group have a similar occurrence distribution with time.

In the simulations, the westerly Iliamna jet is the most frequently occurring strong gap wind in Cook Inlet. The horizontal and vertical structures of this jet are depicted through high resolution numerical modeling of three typical events. These three events are characterized by differing Froude Numbers upstream of the gap. Available SAR-derived wind images are employed to verify the model simulations at the surface. High resolution simulations revealed interesting structures of this gap wind: a small-scale strong wind zone above the seaward edge of the gap, a vertically propagating wave followed by a low-level transition zone in which the wind speed is relatively lower and increases at a relatively slow rate, and a high-speed jet core. The simulation and SAR image show that the jet can extend eastwards horizontally several hundred kilometers off shore. The jet is influenced by several factors. The topography of the gap helps shape the jet outflow, the uneven topography at the seaward end of the gap causes more air flow out through the lower part of the gap. The side wall outside the gap accelerates the jet. The warm ocean actually decelerates the jet. The stability of the atmosphere greatly affects the distance the vertical propagating wave can travel. The more stable the atmosphere, the less distance the wave can travel. The stability of upper level atmosphere layers also influences the strength of the jet. The more stable the upper level atmosphere is, the stronger the jet will be.

Three sensitivity simulations, namely the control run with the original topography, the S_1 run with the barriers in the gap removed, and the S_2 run with the barriers and the sidewall downstream of the gap removed, are conducted to investigate the influences of the extremely complex terrain. The comparison between these simulations shows that the barriers in the gap generate a vertically propagating wave acceleration of the flow in the lee side and actual deceleration of the jet further downstream of the gap. Regardless of whether the flow is supercritical or not, the sidewall on the southern side of the channel constrains and accelerates the gap outflow. When the incident flow is more stable and capped close to the sea surface the acceleration is more obvious. The gap outflow becomes nearly geostrophic when reaching the North Gulf Alaska. However, the fanlike shape does not show up in these cases.

The strong surface winds in the Gulf of Alaska often cause difficulties for the local marine and aviation traffic. The interactions among various flows make the surface wind regime more complicated in this region. High resolution numerical modeling helps understand and forecast these surface winds. Three cases of interacting down-Inlet wind and cross channel easterly wind in the lower Cook Inlet were analyzed. The available corresponding SAR-derived wind image also showed similar strong surface wind patterns. The convergence zone of these two air flows were clearly shown in both RAMS wind and SAR wind despite the difference of spatial resolution. The similarity between results of these two independent sources confirmed the confidences of these two methods in predicting/diagnosing highly structured wind fields.

INTRODUCTION

From the meteorological perspective, the Gulf of Alaska is a region of extremes. Cook Inlet and Shelikof Strait, on the northern periphery of the Gulf, experience the potent consequences of vigorous marine extratropical cyclones making landfall in some of the most dramatic and extreme terrain in North America. The high frequency of storms, on average one every four to five days during the cold season (Hartman 1974), create precipitation extremes of up to eight meters per year of liquid equivalent (Wilson and Overland 1986) in terrestrial sites with favorable orography. Much of the precipitation on land remains impounded (at least temporarily) in the region's many glaciers, but eventually returns to the ocean as a major component of the estimated peak of 60000 m^3 s^{-1} of freshwater discharge (Royer 1981) into the Gulf each fall.

The relative juxtaposition of three climatologically semi-permanent features—Aleutian Low, the East Pacific High and the Siberian High—tend to determine the large-scale meteorological pattern affecting the north Gulf of Alaska coast at any given time (Putins 1966, Overland and Hiester 1980). Along the north Gulf of Alaska coast, terrain plays an important role in determining local weather. During winter months, the high terrain of rugged coastal ranges in southcentral and southwest Alaska isolate the cold continental airmass of interior Alaska from the relatively warmer and moist marine airmass typical of the Gulf of Alaska (e.g. Overland and Bond 1993). Storms moving north and east into the Gulf along the Aleutian storm track become trapped by terrain that at some points exceeds 5000 m (Wilson and Overland 1986). This has several consequences. First, these storms tend to stall and ultimately decay off-shore from Cook Inlet and the Kenai Peninsula through Prince William Sound and on to Yakutat (e.g. Roebber 1984) earning this curved region of coastline the sobriquet "Coffin Corner". Second, the ridge-top pressure difference arising from the disparate airmass temperatures produces an environment conducive to gap and channel winds (Macklin, et al. 1988) which may at times be quite strong, with gusts around 50 ms^{-1}(Reynolds, et al. 1981, Coleman and Dierking 1992, Overland and Bond 1993). Third, the frontal development that occurs near the coast when differing airmasses collide there (Reynolds 1983, Bond and Macklin 1993) can produce mesoscale (sub-Rossby radius) features such as jets, mesocyclones and local wind reversals that are completely undetectable in the larger scale weather patterns.

With the exception of Anchorage and the north Kenai Peninsula, there are few routine atmospheric and oceanic measurements in much of this sparsely settled area. This paucity of observations is also seen on a larger scale, with very few atmospheric soundings "upstream" (i.e., to the south and west) of southcentral Alaska. With the advent of SAR-derived wind retrievals, we have been given very high resolution "snapshots" of the surface atmospheric state. Unfortunately, SAR snapshot images of Cook Inlet/Shelikof Strait are typically only available every few days. From a scientific standpoint, they are of great utility in verifying model simulations but are not adequate for detailed studies of the frequency and duration of LLJ occurrence or the dynamics that produce them. Aircraft-based studies (e.g. Macklin, et al. 1990, Bond and Macklin 1993) also present only snapshots of a few events. Often, mesoscale circulations are poorly represented, if at all, by the current operational weather forecast models. There is a strong need for a modeling capability that can resolve such terrain-induced circulations, both for the immediate value of better guidance for the weather forecaster and more

basically for the ability to understand and explore the phenomena involved on a quantitative level. A high-resolution numerical model that verifies with the available observations (SAR and others) can provide a valuable research and short-term forecast tool for quantifying LLJ structure, duration, causal mechanisms and relationships to larger-scale weather features.

Better understanding of Cook Inlet's weather regimes can help avoid or prevent accidents with catastrophic costs in terms of environmental damage and loss of life. Additionally, the model simulations can act as "integrators" of observations that do exist, by combining observations with short-term simulations to produce high-resolution gridded data sets consistent with both the observations and the fluid-dynamical equations of motion. The resultant data sets can be used by other models (for example, regional ocean models, ecosystem models, etc.) to provide realistic three dimensional atmospheric inputs that are highly resolved in space and time and more accurately represent local terrain influences.

The overall objectives of this study were to develop a capability that is both fast and efficient enough to act as a nowcast/forecast system, versatile enough to be used for a variety of research purposes, and stable enough to produce reliable gridded data sets for input to other models, and use this capability to systematically study LLJ phenomena in Cook Inlet and Shelikof Strait. This work includes:

- Developing an ongoing archive of simulated gridded surface winds, temperature, and precipitation at high resolution,
- An evaluation of the predictability of LLJ occurrence, strength and duration, and validation of numerical simulations wherever possible,
- Developing an understanding of the underlying mechanisms that drive LLJs in this region,
- A climatology of LLJ occurrence and likelihood in several wind-prone locations as determined by the model simulations and available observations,
- A study of the vertical and thermal structure of wind jets, and
- A study of local cloud fields and precipitation associated with LLJs.

METHODS

We used the parallel computing capability being developed at AEFF (at Merrill Field in Anchorage, Alaska) and the RAMS to create this modeling capability. The model output is validated against satellite and buoy observations.

Computing Facility

The computing facility in AEFF is a new high performance computer cluster which consists of 15 Dell poweredge dual Xeon 3 Ghz computers. These computers are connected using Gigabit Ethernet to form a high performance Beowulf parallel computing system.

Model Description

The mesoscale model used in this study is the Regional Atmospheric Modeling System, developed at Colorado State University and Mission Research Corporation. RAMS is a multipurpose numerical simulation system (Pielke, et al. 1992a, Cotton et al. 2002). RAMS is a nonhydrostatic primitive-equation, finite-difference model that includes parameterizations for mixed-phase microphysics, radiation, and planetary surface processes. It is most frequently used to simulate atmospheric phenomena on the mesoscale (horizontal scales from 2 km to 2000 km) for applications ranging from operational weather forecasting (Cotton et al. 1994) to air-quality regulatory applications (e.g. Pielke, et al. 1992b, Uliasz, et al. 1996) to support of basic research (e.g. Olsson and Cotton 1997a, Olsson and Cotton 1997b, Olsson, et al. 1998).

One of the strengths of RAMS is its versatility and applicability to a wide range of geophysical and hydrodynamic phenomena. The code contains a variety of structures and features including nonhydrostatic codes, resolution ranging from less than a meter to hundreds of kilometers, domains from a few kilometers to the entire globe, and a suite of physical options (Cotton, et al. 2002). RAMS provides a wide range of options that allow it to be tailored for a broad spectrum of applications. RAMS has been successfully used at very high resolutions to simulate boundary layer eddies with 10-100 m grid spacing, (e.g., Stevens, et al. 1998a, Stevens, et al. 1998b, Olsson and Harrington 1999, Olsson and Harrington 2000). RAMS has been used with grid-spacing of a few kilometers to simulate seasonal-long precipitation processes (Copeland, et al. 1996, Pielke, et al. 1999a, Pielke, et al. 1999b, Liston and Pielke 2000). RAMS has also been used with grid-spacing of ~100 km for multi-season hemispheric climate simulations.

Central to the versatility of RAMS is a multiple grid-nesting scheme (Figure 1) that permits solution of the primitive equations simultaneously on any number of interacting computational meshes of differing spatial resolution, using physics appropriate to the scale being considered, while maintaining physical and numerical consistency across all grids. The highest resolution mesh is used to model details of small-scale atmospheric systems. Coarse meshes are used to model the synoptic environment of these smaller systems and provide boundary conditions for the fine-mesh regions of interest. This multi-scale capability is very important in the greater Cook Inlet region where the synoptic scale pressure gradients and associated weather systems interact strongly with local terrain to procedure quite localized and highly ageostrophic near-surface circulations.

For this study, grid 1 has 50 by 50 grid points with a grid spacing of 64 km, sufficient to capture the synoptic-scale storm events. Grid 2 has 74 by 70 grid points with a spacing of 16 km, and grid 3 has 122 by 134 grid points with a spacing of 4 km (Figure 1). Grid 3 covers the entire area of Cook Inlet and Shelikof Strait and is the focus of the analysis for this study. Vertically, all the three domains have the same 36 levels. The vertical grid spacing starts at 50 m at the surface and stretches by a factor of 1.15 for each successive level above the surface, to a maximum separation of 1200 m. This gives a vertical domain height of 23.5 km above mean sea level, which encompasses the troposphere (where most weather events occur), the tropopause, and the lower stratosphere (e.g. Wallace and Hobbs 1999). The sea surface temperature (SST), land and vegetation, and topography data are from the standard RAMS data sets.

Figure 1. The RAMS domains for Cook Inlet and Shelikof Strait. G1 has a grid spacing of 64 km, G2 16 km, and G3 4 km.

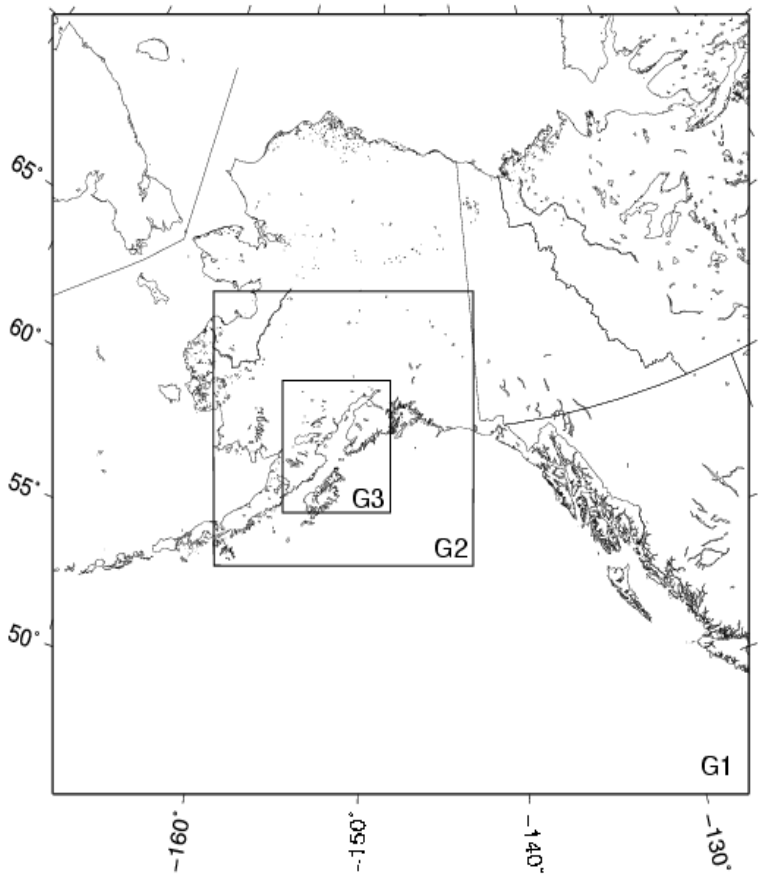

To keep both the mountain heights and the deep valley effects on circulations in each domain, the "reflected envelope orography" scheme (Walko and Tremback 2002, Marty, et al. 2000) is used. The digital elevation model (DEM) used here is at 30-second resolution. The Harrington scheme (Harrington, et al. 1999) is used for radiation calculations and is updated every 1200 seconds. The coarse grid time step is 60 seconds. The integration results are written every hour. The 45-km ΔX analysis and forecast data from the NCEP Eta forecast model (WMO 216 grid) are used as the initial and lateral boundary conditions respectively. The model is operationally run daily in a 36-hour forecast mode. Although many meteorological elements are accessible from the model simulation, we focus on the near-surface wind field here.

Topography of Cook Inlet and Shelikof Strait

Figure 2a gives a two dimensional image showing the location of mountain ranges, channels and water bodies of Cook Inlet and Shelikof Strait region. Most of the mountain ranges are between 600—2000 m. Turnagain Arm, Tuxedni Bay, Iliamna Lake, Kaguyak and Puale Bay are marked with texts. These places have elevations below 600 m which is much lower than surroundings. They are the locations of gaps through which gap winds frequently blow. Cook Inlet is bounded on the west by the massive Aleutian Range and on the east by the Chugach and Kenai Peninsula mountains. Shelikof Strait has Alaska Peninsula on the west and Kodiak Island on the east. During the winter storm season, strong atmospheric pressure gradients occur across this region as cyclones transit the north Gulf. These pressure gradients are one of the main factors inducing strong wind events in this region. Figure 2b is a three dimensional perspective of the topography of the areas of interest. It depicts the variations of the elevation of these places. The perspective angle was chosen to show the pass way of major wind jets. Besides the channels, the gap at Iliamna Lake and Puale Bay vicinity are clearly visible. The outstanding high terrain in the northwest corner of the figure is the Denali massif which has an elevation over 5000 m ASL.

Figure 2. Topography of Cook Inlet and Shelikof Strait in two dimensions (a) and three dimensions (b).

a)

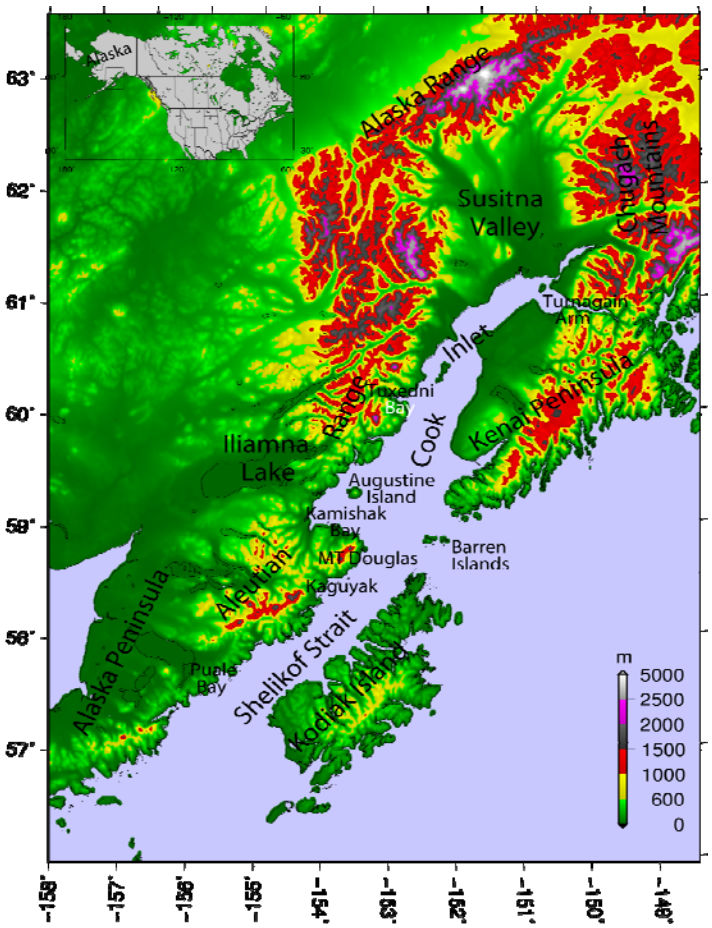

b)

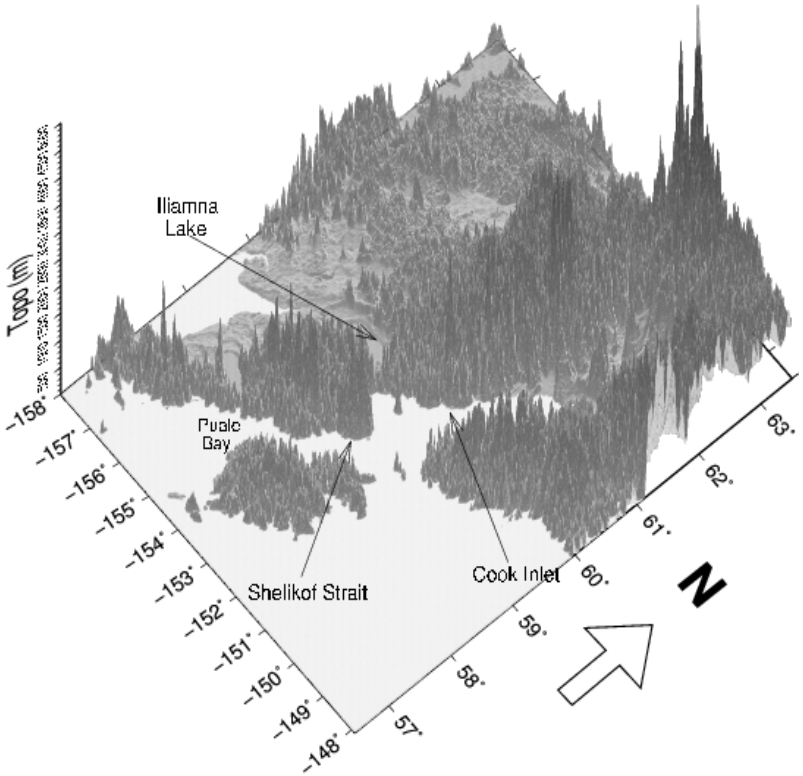

RESULTS AND DISCUSSION

Verification of RAMS wind simulations in Cook Inlet and Shelikof Strait

Grid-to-observation

When the station observations are used, two verification approaches can be employed: grid-to-observation-point (G-P) and observation-point-to-grid (P-G) (Tustison, et al. 2001). G-P is good for data sparse regions such as Alaska. There are only a few C-man and buoy stations in the Cook Inlet and Shelikof Strait region (Figure 3). Meteorological observational data from these stations were collected for verification purposes. A bi-linear algorithm is used for grid-to-observation interpolation.

Figure 3. C-man and buoy stations in Cook Inlet and Shelikof Strait.

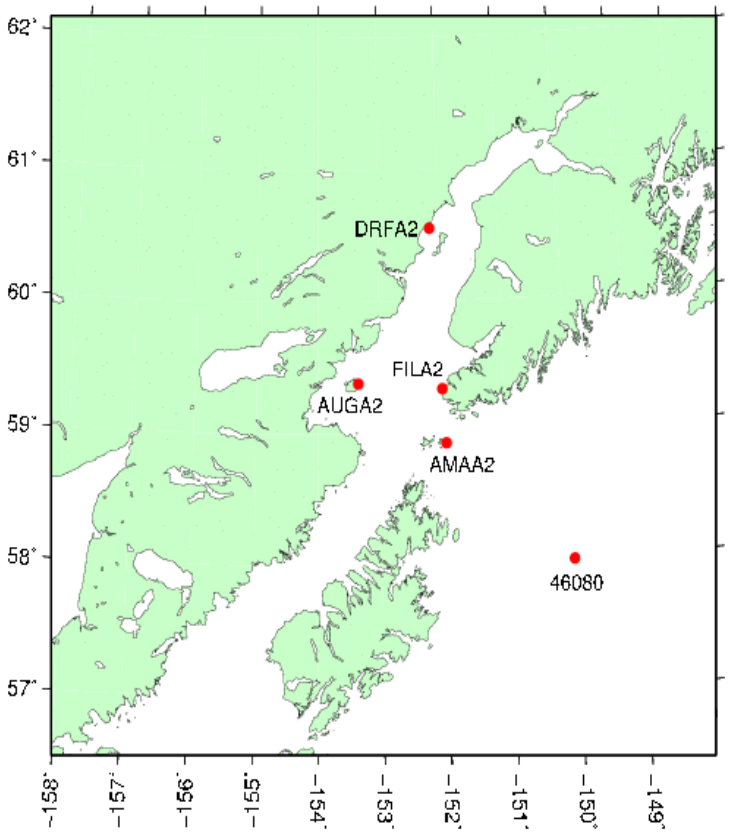

The statistical measures used to quantify model forecast errors are the bias (forecast – observation), root-mean-square (rms) error, and error standard deviation (std). For interpretation of results, it is helpful to recognize that the total model error includes contributions from both systematic and nonsystematic sources. Systematic errors (model biases) are usually caused by a consistent misrepresentation of such factors as orography, radiation, and convection. Nonsystematic errors are indicated by the error standard deviation and represent the random error component caused by initial condition uncertainty or inconsistent resolution of scales between the forecasts and observations. While it is possible to partially correct for known systematic errors by subtracting the bias, the nonsystematic errors are rather unpredictable in nature and may contribute to a degraded daily forecast product (Nutter and Manobianco 1999).

If Φ represents any of the parameters under consideration for a given time, then forecast error is defined as $\Phi' = \Phi_f - \Phi_o$, where the subscripts f and o denote forecast and observed quantities, respectively. Given N valid pairs of forecasts and observations, the bias is computed as:

$$\overline{\Phi'} = \frac{1}{N}\sum_{i=1}^{N} \Phi'_i \qquad (1)$$

The rms error is computed as:

$$rmse = \sqrt{mse} = \left[\frac{1}{N}\sum\left(\phi_i'\right)^2\right]^{1/2} \qquad (2)$$

The std is computed as:

$$\sigma = \left[\frac{1}{N}\sum_{i=1}^{N}\left(\phi_i' - \overline{(\phi')}\right)^2\right]^{1/2} \qquad (3)$$

The mean square error (mse) can be decomposed (Murphy 1988, Nutter and Manobianco 1999) as follows:

$$mse = \overline{\Phi'}^2 + \sigma'^2 \qquad (4)$$

Therefore, the total model error consists of contributions from model biases $\overline{\Phi'}^2$ and random variations in the forecast and/or observed data. Note that if the model bias or systematic error is small, most of mse is due to random, nonsystematic type variability in the errors.

The surface wind bias, rms and std are calculated for each C-man and buoy station. The averages were calculated over 5 days, 10 days, 30 days and 60 days. Both wind direction and speed show reasonably good agreement with the observations for most periods, though results vary with season and location. (It should be noted that the winds are measured at various heights—typically 5 or 10 m—depending on observation platform, but all are being compared to the modeled 23.5 m lowest level winds). An example of the method results can be found in Figure 4.

There is no doubt that grid 2 (16 km) and 3 (4 km) have more skills than grid 1 (64 km) in terms of objective and subjective verification. Grid 3 (4 km) has advantages over grid 2 because it has higher horizontal resolution and is able to resolve more details of the topography which affects the weather. In some instances however, the finer grid (grid 3) may not show skill over that of the coarser grid (grid 2) in objective verification and the added value by the finer grid may not always be clear. For example, verification over the C-man station in Augustine Island (AUGA2, see Figure 4) shows that grid 2 is slightly better than grid 3 in this case.

Figure 4. Verification over the C-man station at Augustine Island for February and March 2004. The left column is grid 2 and the right grid 3. The vertical axes are wind direction and speed. The horizontal axis is forecast hours. Zero hour is the model initial time and 36 hour is 36 hours away from the initial time. The bias is calculated for 5, 10, 29 and 60 days respectively starting from 1 Feb 2006.

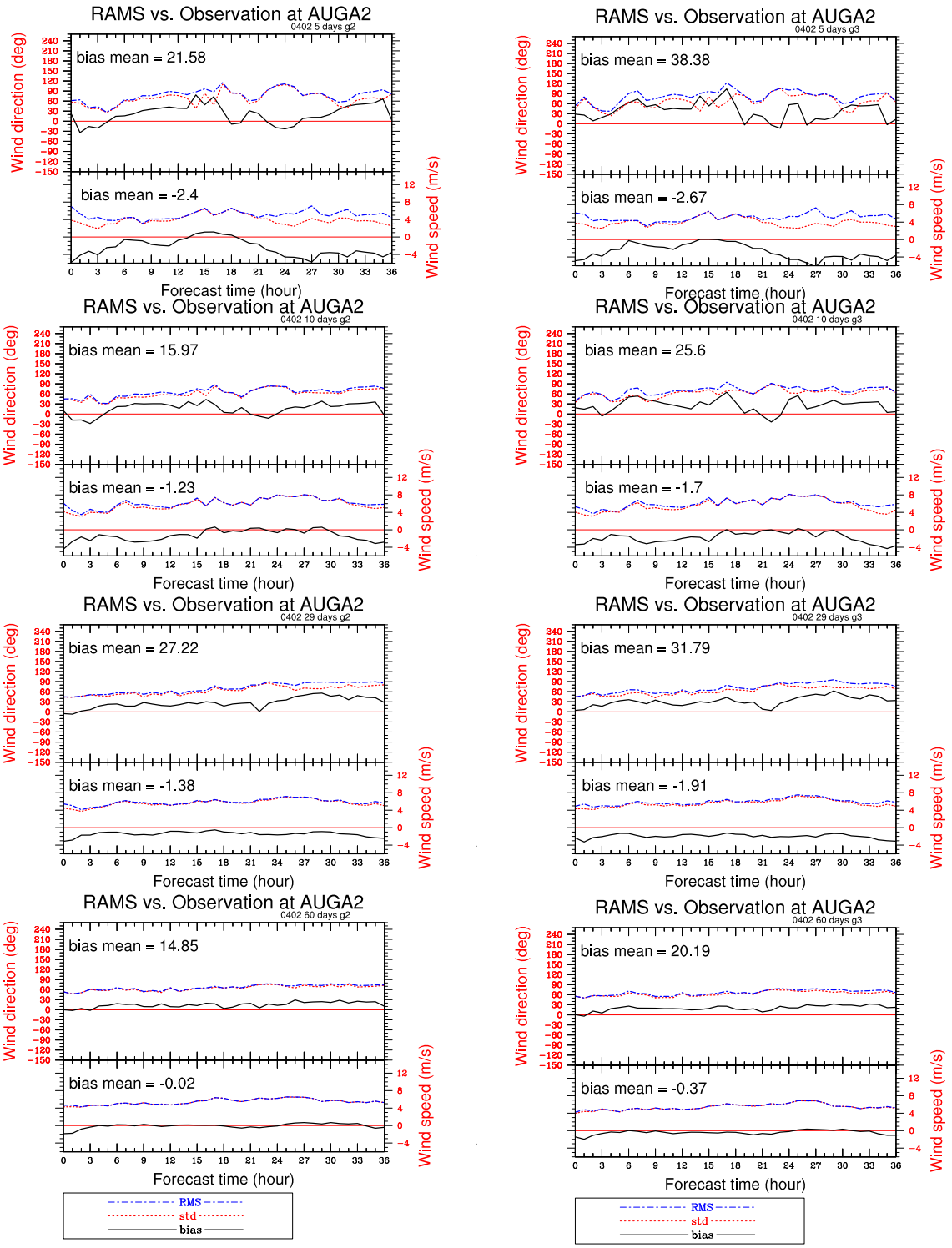

Verification against SAR-wind image

The Synthetic Aperture Radar provides a snapshot of the surface winds over water bodies (Monaldo, 2000). For this study, a collection of a year of SAR-derived wind images of the Cook Inlet and Shelikof Strait was obtained from the Johns Hopkins University Applied Physics Laboratory (http://fermi.jhuapl.edu/people/winstead/_web_wind_NSF/index.html). The intermittent nature of the temporal SAR coverage does not permit systematic verification of the RAMS hourly forecasts. However, it does supply an independent source for qualitatively evaluating the model simulations. The available SAR-derived wind images corresponding to various wind jets and the corresponding simulated surface wind images show a good agreement. We will not show all of these pairs of images under the consideration of making the report concise. Some samples of these SAR-wind images will be shown later.

Low-level wind jet regimes and climatology

Through the examination of the simulated surface winds, 10 frequently appearing wind regimes are recognized (Figure 5). These wind jets are classified into 10 different categories according to their location and orientation: the Turnagain Arm (TGA), Tuxedni Bay (TNB), Cook Inlet up channel (CIu), Cook Inlet down channel (CId), Iliamna (ILA), Iliamna reversed (ILAr), Kaguyak(KGY), Shelikof up channel (SKFu), Shelikof down channel (SKFd) and the Puale Bay (PUB) jet. They are further divided into four general groups according to wind direction: cross-channel westerly, easterly, and up and down Inlet flows. The westerly includes ILA, KGY, PUB and TNB; the easterly includes ILAr and TGA; the down channel includes CId and SKFd; the up channel includes CIu and SKFu.

Figure 5. Schematic of the low-level wind jets in Cook Inlet and Shelikof Strait. The arrows indicate the locations and directions of the jets. A jet may occupy the whole channel where the arrow indicates.

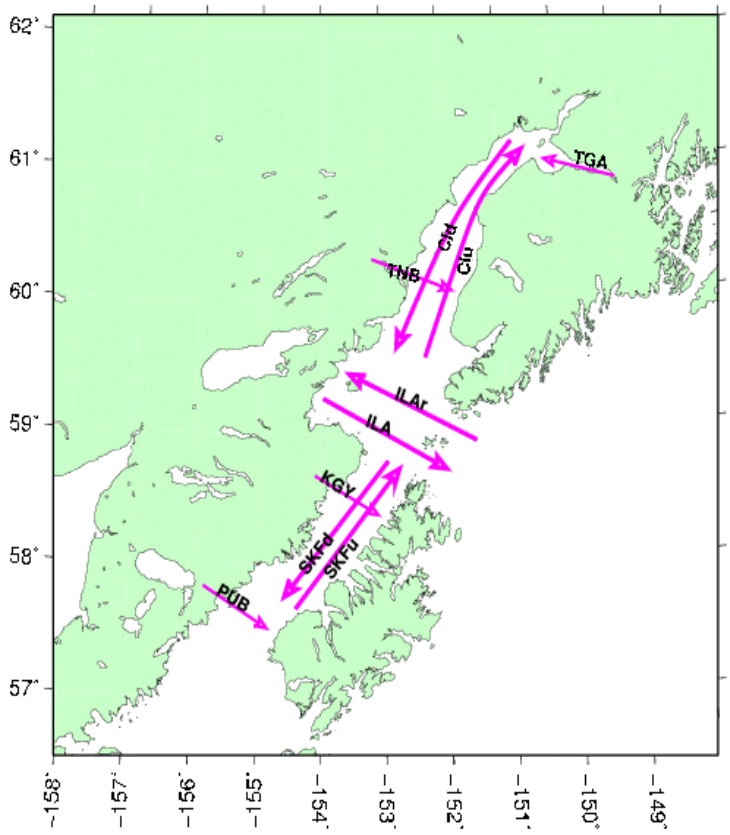

Table 1. The full name of abbreviations of various jets in Cook Inlet and Shelikof Strait.

Jet	Full name of the jet
TGA	Turnagain Arm jet. Strong easterly gap wind from the Turnagain Arm.
TNB	Tuxedi Bay jet. Strong westerly gap wind from the Tuxedi Bay.
CId	Down channel Cook Inlet jet. Strong northeasterly wind along the Cook Inlet.
CIu	Up channel Cook Inlet jet. Strong southwesterly wind along the Cook Inlet.
ILA*	Strong westerly wind in the low Cook Inlet, originating from the major gap in the Aleutian Range, east to the Iliamna Lake.
ILAr	Strong easterly wind in the low Cook Inlet, originating from the Kennedy/Stevenson Entrance.
KGY	Strong westerly wind from the gap in the Aleutian Range in the Kaguyak.
SKFd	Down channel Shelikof Strait jet. Strong northeasterly wind along the Shelikof Strait.
SKFu	Up channel Shelikof Strait jet. Strong southwesterly wind along the Shelikof Strait.
PUB	Strong westerly wind from the Gap in the Aleutian Range east to the Becharof Lake.

* Also referred as Kamishak low level jet (e.g. Macklin, et al. 1990).

Systematic analysis of the resulting simulated low-level wind field makes it possible to characterize these jets and gap flows in spatial and temporal detail. The jets often, though not always, occur in discrete groups. The westerly jets are frequently concurrent though ILA occurs most frequently. The westerly and easterly normally do not co-exist. The jets along the larger major channels- Cook Inlet and the Shelikof Strait- (CIu, CId, SKFu and SKFd) can result from either strong pressure gradients along the gap (highly ageostrophic) or the channeling of large-scale flow (supergeostrophic). When the pressure gradients are over 1 mb per 50 km along the Inlet/Strait, there are along-channel jets occurring anti-parallel to the pressure gradients. Note that the same pressure gradients *across* the channel may not necessarily induce cross-channel jets when the background flow is very strong. Instead along-channel jets may be induced.

For the 2003 to 2004 winter (Figure 6), about 65% of ILA is accompanied by KGY, 61% of ILA has PUB occurring at the same time. TNB is the least frequent jet, due to its large threshold pressure gradient. About 10% of ILA occurs with TNB. All KGY and TNB are concurrent with ILA. About 89% of PUB occurs with ILA. The most frequently occurring jet is the ILA which occurs almost one third of the days.

For the 2004 to 2005 winter (Figure 7), the most frequently occurring jet is the ILAr, followed by the SKFu, TGA and CId. TGA and CId have similar occurrence pattern during this season. The reason is that the strong easterly TGA is often blocked by the Cook Inlet western bank with very high elevations which forces the air to flow down the inlet along the pressure gradient. Most SKFu is induced by the lows traversing through the North Gulf of Alaska and it is likely to occur when the low is centered at western Alaska.

In the 2005 to 2006 winter (Figure 8), ILA is the most frequently occurring jet again. The westerly jets are much more frequent than the easterly and the along channel jets. In this season, the traversing lows more frequently take an east-wards course. In the mean time, the ridge over the western Alaska often builds and sustains forming a strong eastwards pressure gradient which drives strong westerly jets in the Cook Inlet and Shelikof Strait.

Figures 6, 7 and 8 show that the occurrence of a jet varies largely from month to month for 2003-2004, 2004-2005 and 2005-2006 cold seasons. There is no particular month favoring all of these jets. For example, ILA occurred most in December 2003 but least in December 2005. The occurrence of a jet also fluctuates significantly from year to year, e.g. ILA occurred 83 times in 2003-2004 winter, but 67 times in 2004-2005 and 100 times in 2005-2006 winter. The duration of a jet also varies within the season and from year to year. For an example, most of TGA lasted less than 6 hours in October 2004 but more have a duration from 9 to 12 hours in January 2005. However, most ILA lasted more then 18 hours for all three winters considered here. This is indeed the predominant LLJ in the Cook Inlet region-- in size, duration, and occurrence-- and is thus the major focus of the analysis presented later in this report.

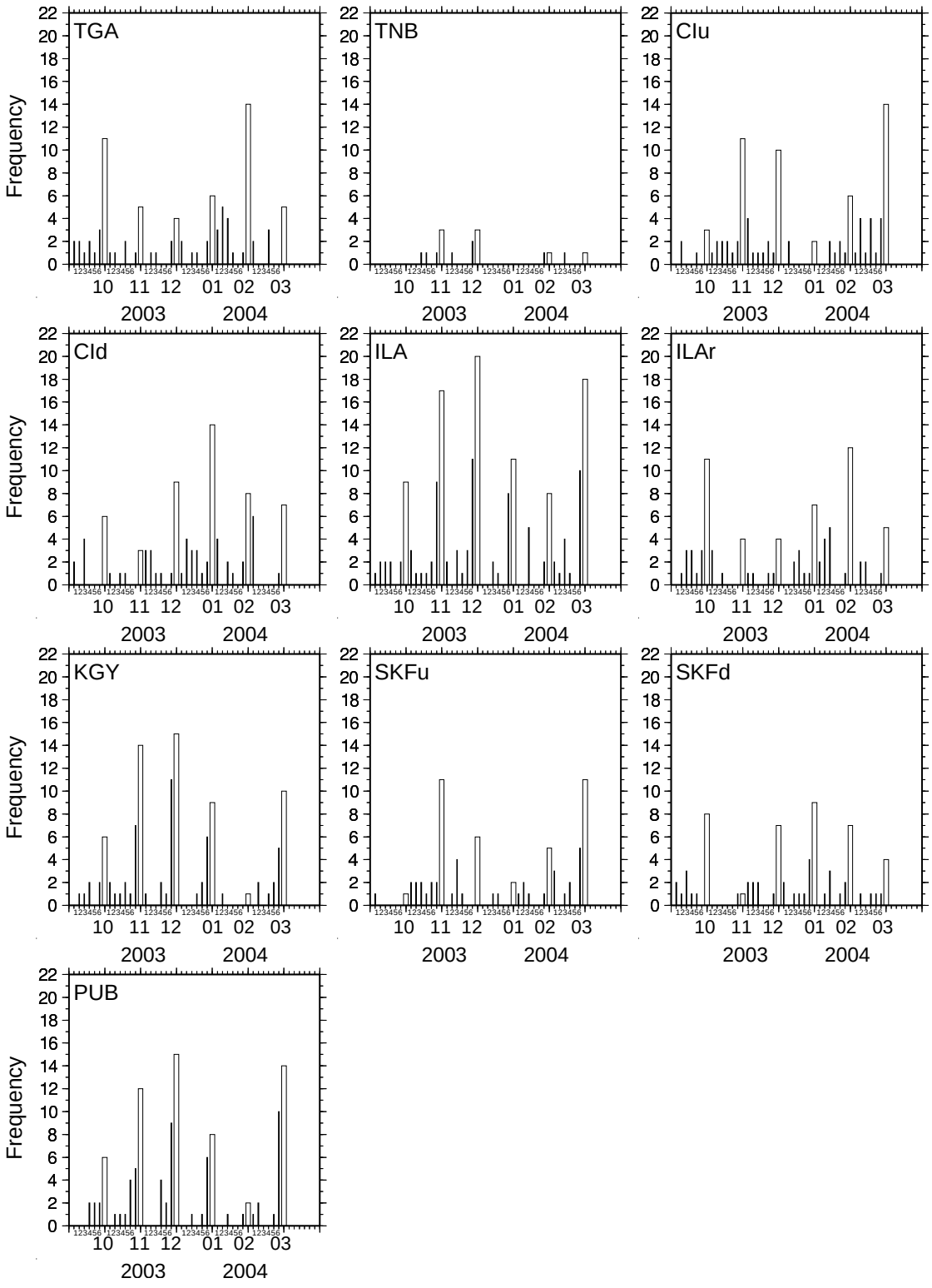

Figure 6. Frequency of low-level wind jets for the 2003 - 2004 winter. The vertical axis is the number of days having wind jets. The horizontal axis has two variables: jet duration category and month. The number 1-6 denotes the 6 category of duration time from less than 6 hours to over 18 hours with a 3 hours interval. The vertical box shows the jet occurrence frequency in each month.

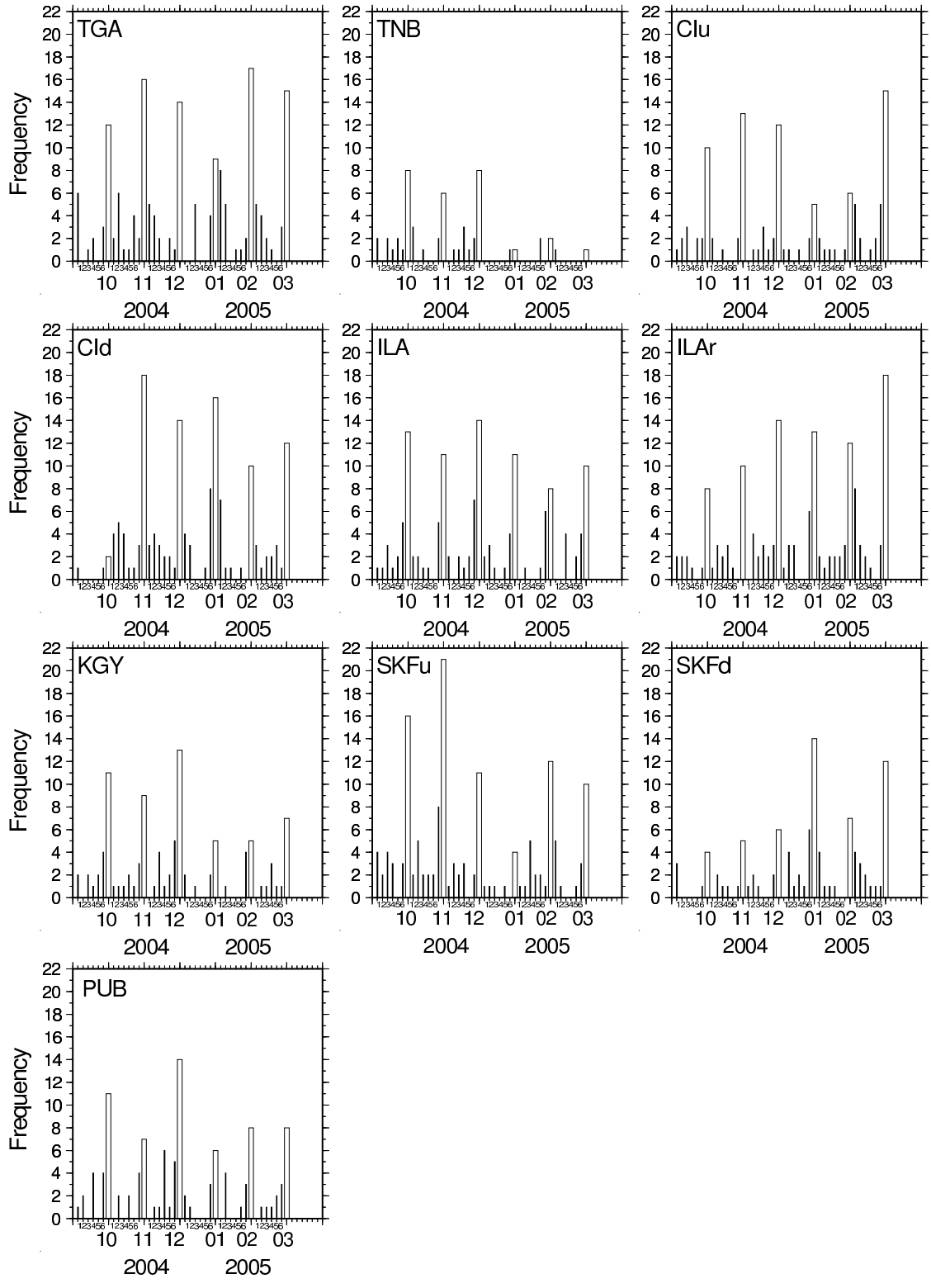

Figure 7. Same as Figure 6 but for the 2004 - 2005 winter.

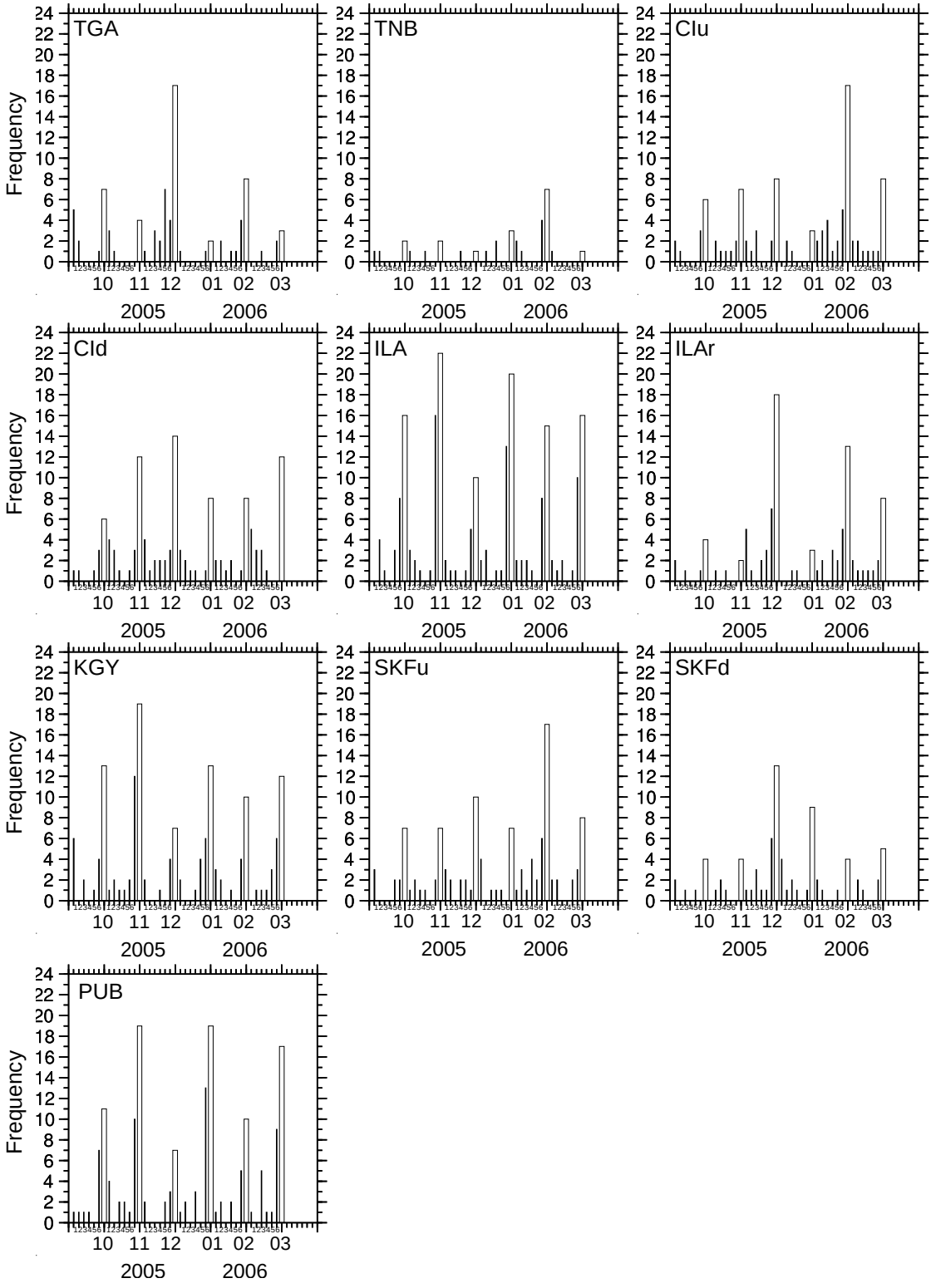

Figure 8. Same as Figure 6 but for the 2005 - 2006 winter.

Structure of ILA jet

The westerly Iliamna jet is the most frequently occurring strong gap wind in Cook Inlet, Alaska. The horizontal and vertical structures of this jet are depicted through high resolution numerical modeling of three typical events (case A on 28 October 2003, case B on 26 November 2003, and case C on 06 February 2004). These three events are characterized with different Froude numbers upstream of the gap. Available SAR-derived wind images are employed to verify the model simulations (see Figure 9).

The Froude number:

$$Fr = \frac{u}{NH}$$

is related to tendency for a flow to be constrained to horizontal plain, where u is horizontal wind speed, N is the buoyancy frequency (related to the vertical thermal stability of the atmosphere) and H is the height of the obstacle. If Fr is small ($Fr<1$), the low-level flow is largely blocked, except where it can flow around the obstacle or through gaps. When $Fr\geq 1$, the flow tends to cross the barriers. Since H is fixed in a given location, the likelihood of the flow to pass over barriers rather than to be forced through the gaps is determined by near-surface wind speed and low-level atmospheric thermal structure.

Figure 9. Comparison of RAMS-wind and SAR-wind. a, b and c show RAMS winds for the 3 cases; a', b' and c' are the SAR-derived wind snapshot for these cases respectively.

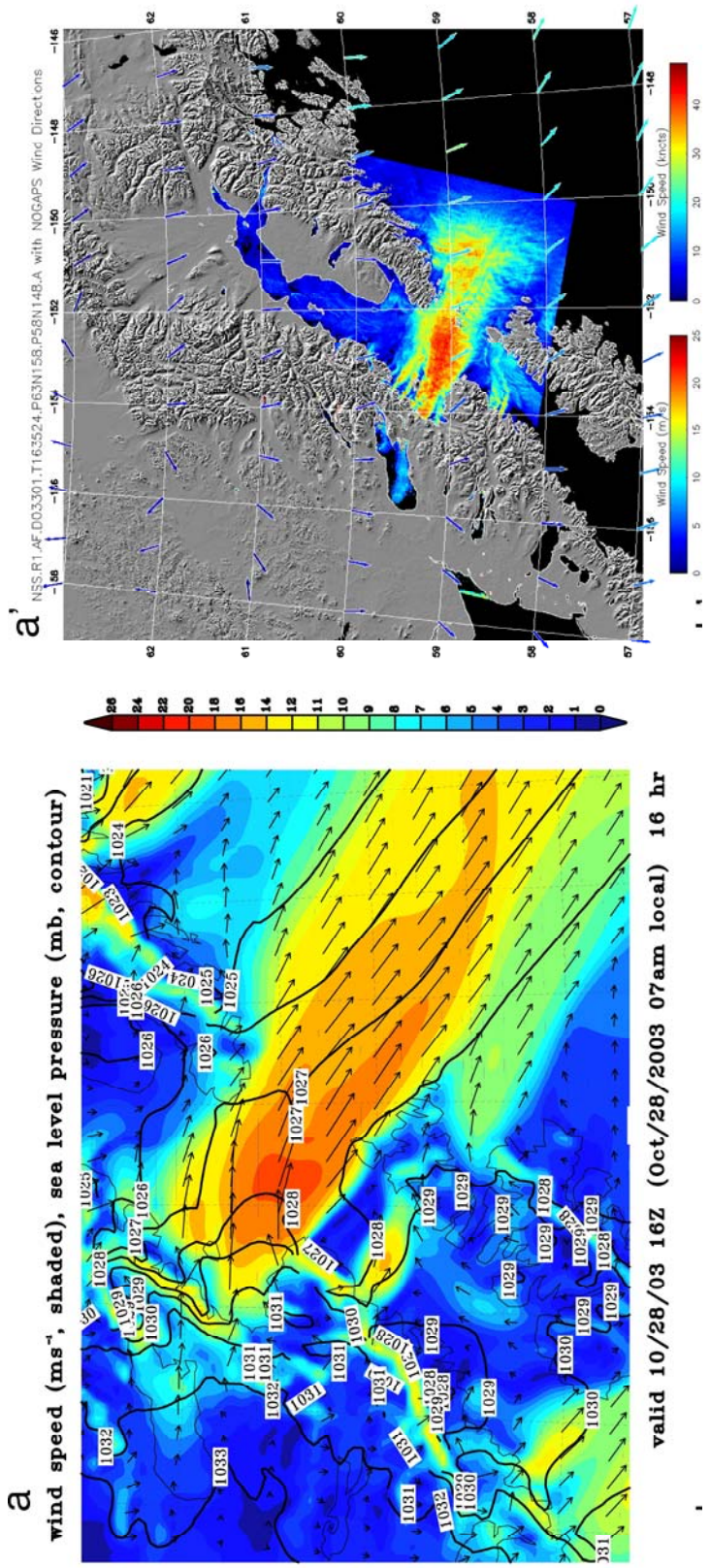

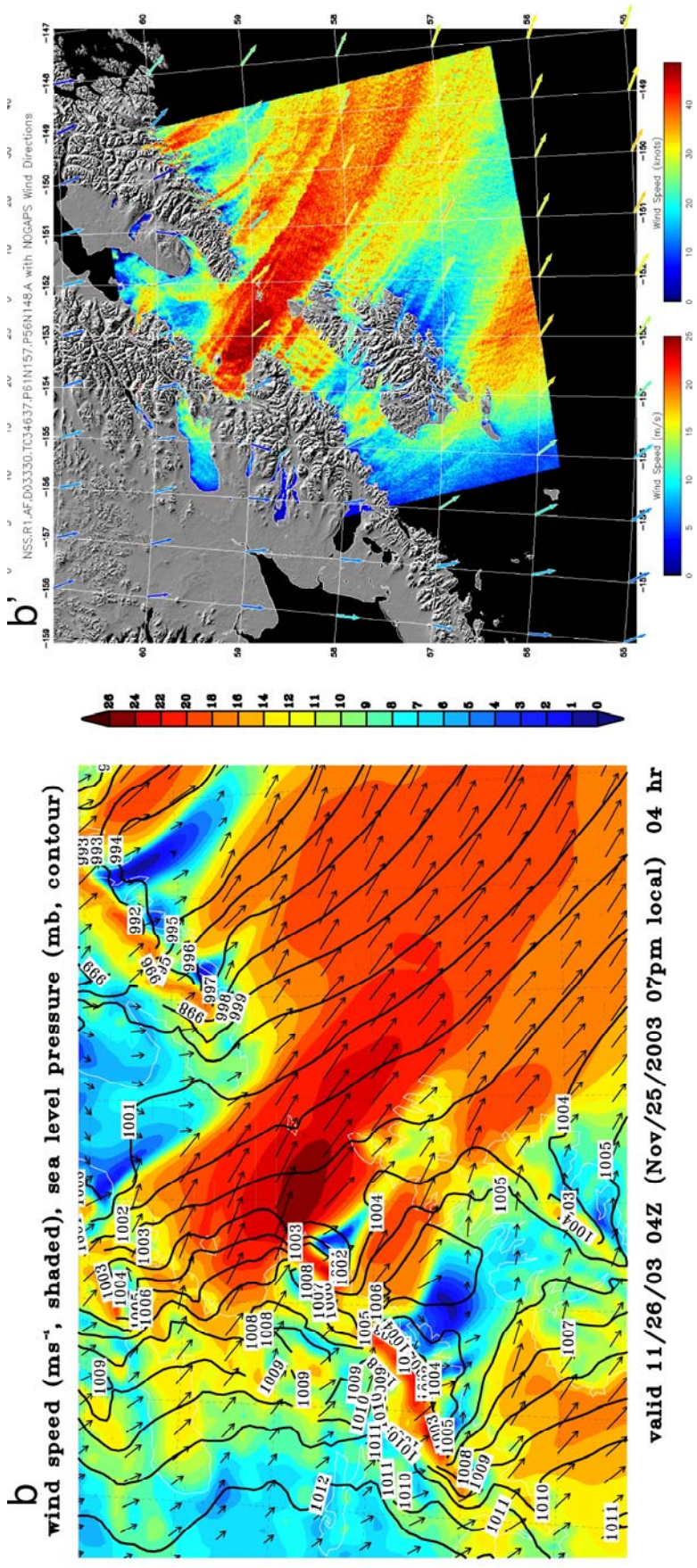
b
wind speed (ms⁻¹, shaded), sea level pressure (mb, contour)
valid 11/26/03 04Z (Nov/25/2003 07pm local) 04 hr
b'
NSS.R1.AF.D03330.T034637.P61N157.P56N148.A with NOGAPS Wind Directions
Wind Speed (m/s)
Wind Speed (knots)

C

wind speed (ms^{-1}, shaded), sea level pressure (mb, contour)

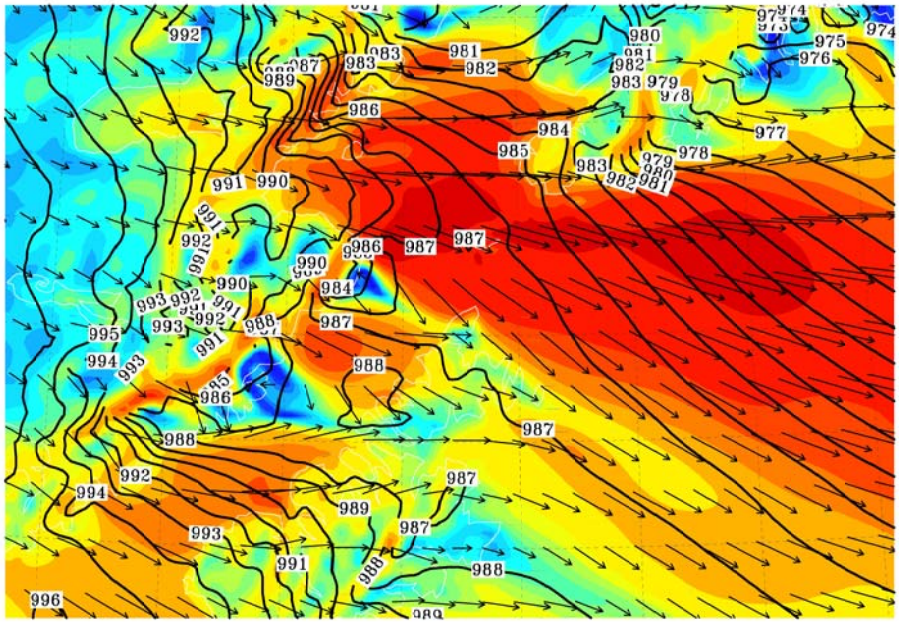

valid 02/06/04 04Z (Feb/05/2004 07pm local) 04 hr

C'

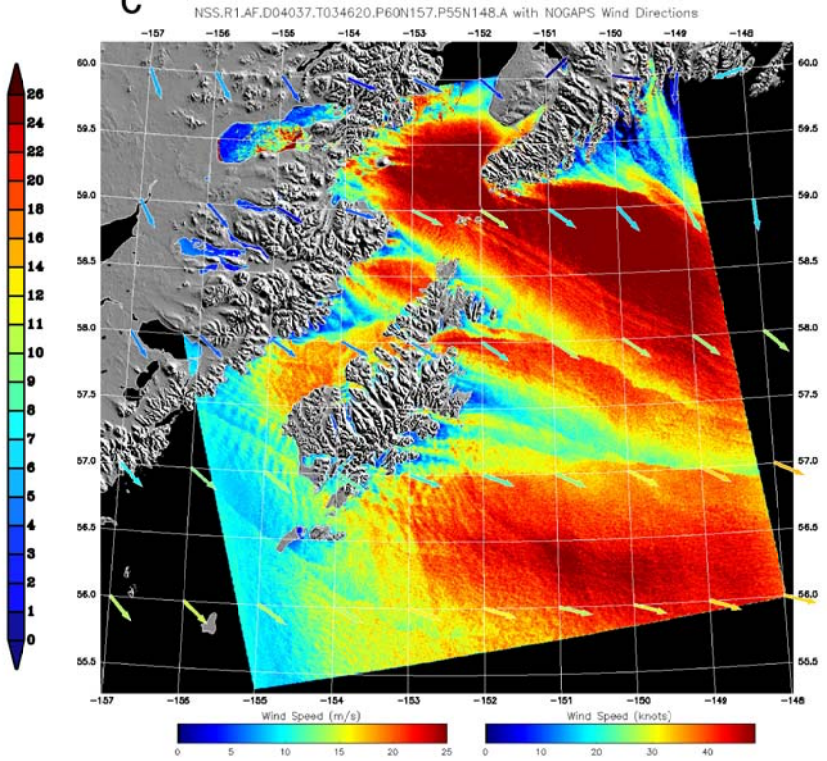

The ILA jet occurs at a topographically complex region often traversed by low pressure systems. The local winds are greatly shaped by the terrain and the imposed pressure system. The ILA jet occurs under the following certain synoptic configurations: low pressure systems traversing through the North Gulf of Alaska, and/or a high pressure system dominating the west Alaska continent. The duration of the presence of a sufficient pressure gradient over the lower Cook Inlet determines the duration of an ILA jet event. When the traversing system moves rapidly, the jet event will have a short life. For quasi-stationary pressure patterns, the jet can last for more than a day, e.g., case A lasted from 02 UTC 28 October 2003 to 02 UTC 29 October 2003; case B lasted from 12 UTC 25 November 2003 to 19 UTC 27 November 2003; and case C lasted from 18 UTC 05 February 2004 to 6 UTC 7 February 2004. During each of these events, strong pressure gradients with a west/east orientation were maintained.

Although the jet is primarily controlled by the synoptic pattern and may last more than 24 hours, it may also have diurnal variations. Typically, the diurnal variation of a surface or low level meteorological variable is induced by the diurnal variation of surface thermal heating which is typically stronger during the day and vanishing or negative at night. Figure 10 shows the maximum surface wind speed at the jet core. Apparently, the diurnal variation exists in all three cases, with peak at around local midnight to early morning. The magnitude of this diurnal variation is significant, it is 5, 10 and 6 ms^{-1} for case A, B and C respectively.

ILA jet simulations

High resolution simulations revealed interesting structures of this gap wind: a small scale strong wind zone above the seaward edge of the gap, a vertically propagating wave followed by a low level transition zone in which the wind speed increases at a relatively slow rate, and a high speed jet core. The simulation and SAR image show that the jet can extend eastwards horizontally several hundred kilometers off shore. The jet is influenced by several factors. The topography of the gap helps shape the jet outflow, the uneven topography at the seaward end of the gap causes more air flow out through the lower part of the gap. The side wall outside the gap accelerates the jet. The orientation of the jet is aligned well with the incident flow. The warm ocean actually slows down the jet. The stability of the atmosphere greatly affects the distance the vertical propagating wave can travel. The more thermally stable the atmosphere, the less distance the wave travels. The stability of upper level atmosphere layers also influences the strength of the jet. The more stable the upper level atmosphere, the stronger the jet

Figure 10. Wind speed at the surface in the jet core. The three cases are marked with triangles, plus signs and circles. The horizontal axis is forecast hour from 00Z, the vertical axis is wind speed (ms^{-1}).

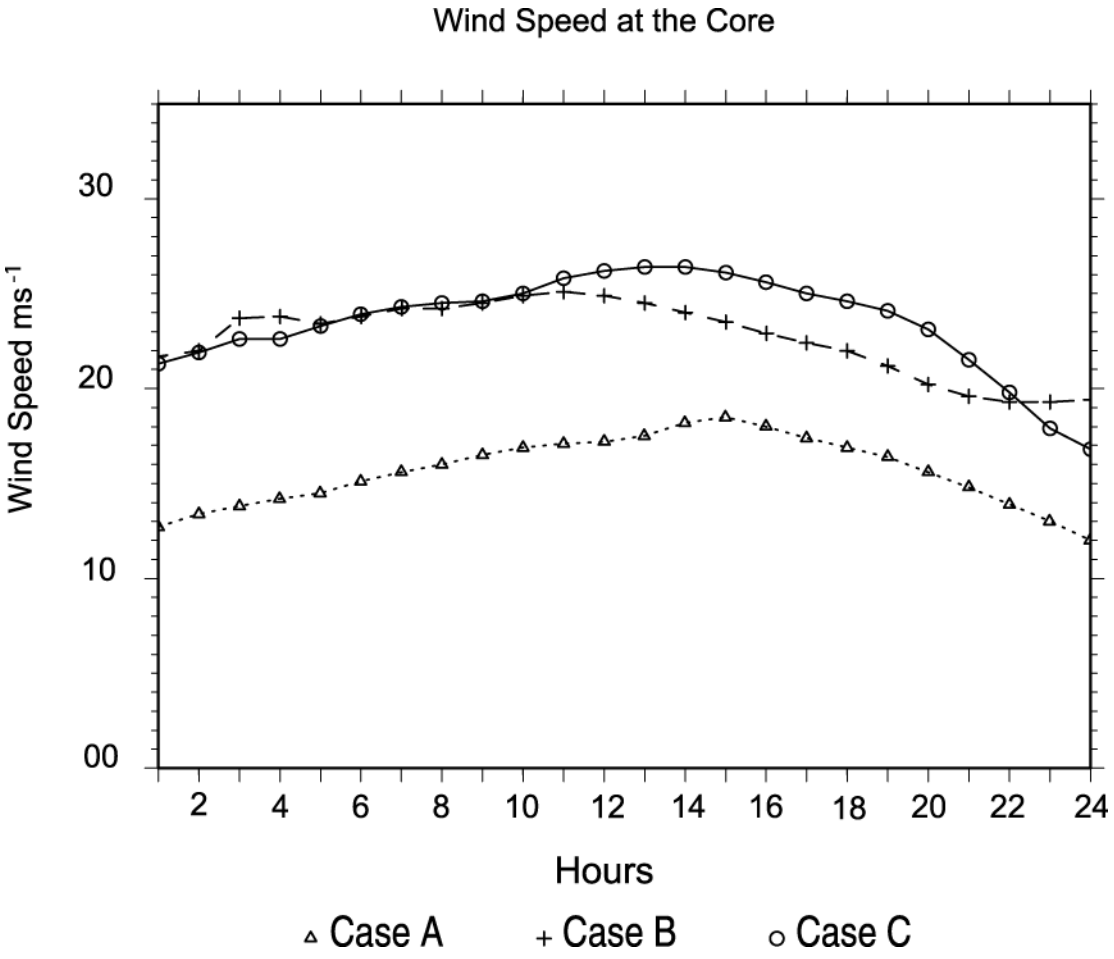

Another common feature of these jets is the high speed core downstream of the sidewall and gap which may be explained by the shallow-water theory of supercritical channel flow (Haack, et al. 2001), since the outflows of these jets are bounded under an inversion and have $Fr > 1$. The expected downwind values of marine layer wind speed and height are determined from conservation of mass and momentum and use of the Bernouli theorem, which states that the total energy along a streamline is conserved. For shallow water flow the Bernouli constant is given by $B = h + v^2/(2g')$, where $g' = \Delta\theta/\theta$ is reduced gravity, h is the marine layer height, and v is the horizontal velocity of the marine layer. Knowing the upstream h, v and g' and downstream h, and g', the downstream v can be estimated. Ideally, $\Delta\theta$ often is represented by a first-order discontinuity, however for a continuously stratified coastal marine layer, determination of the inversion is more ambiguous. We estimated the inversion base from the lowest level for which the potential temperature gradient is greater than 0.02 K m^{-1}, and the inversion top by the height at which the gradient again falls below 0.02 K m^{-1}. The layer depth is taken as the height midway between inversion base and top, and the inversion strength $\Delta\theta$ is the difference between the

potential temperature at the inversion top and the average mixed layer potential temperature. Table 2 gives $\Delta\theta$, θ, h and v for the jet. It shows that the jet core speed estimated using the shallow-water theory is lower than simulated by the model. This is because the mesoscale model simulates the jet in a more sophisticated way, while the shallow-water theory of supercritical channel flow assumes that the marine layer upstream of the characteristic wave is uniform, steady state, inviscid, vertically bounded, and pressure is constant along the wave. This is highly simplified considering the complexity of the flow in the lower Cook Inlet region. More important, there is a pressure gradient upstream of the jet core for each of these cases and it has a significant component directed downstream. Consequently, the flow speed is higher than that predicted by shallow-water theory, though that theory does account for most of the acceleration of the flow downstream of the sidewall.

Table 2. Parameters for characterizing supercritical flow using shallow-water theory. h_1, $\Delta\theta_1$, θ_1, v_1 and Fr_1 are the marine layer height, potential temperature difference across the inversion, potential temperature, wind speed and Froude number for the upstream flow midway from the coast to the starting point of the jet core. h_2, $\Delta\theta_2$, θ_2 and v_2 are for the jet core. v_{2w} is the flow speed estimated via the shallow-water theory.

Case	h_1 (m)	$\Delta\theta_1$ (K)	θ_1 (K)	v_1 (ms^{-1})	Fr_1	h_2 (m)	$\Delta\theta_2$ (K)	θ_2 (K)	v_2 (ms^{-1})	v_{2w} (ms^{-1})
A	600	4	275	16	1.7	400	4	276	19	18
B	850	3	266	23	2.4	750	3	267	27	23
C	850	4	266	22	1.5	550	4	268	25	24

The direction of the incident flow influences the orientation and location of the jet core (the portion of the jet coincident with the speed maximum).For example, case A and B have a more southward incident flow thus the jet core is more South-North oriented, and the center of the jet core is in the south side of the LCI.

Sensitivity to microphysics scheme, clouds and the temperature gradient between the sea surface and the lower atmosphere

During winter, air from Alaska's interior is cold and dry, but the ocean is relatively warm. Therefore, there exist strong temperature and moisture gradients, and accompanying fluxes, between the sea surface and the gap flow. To investigate the impact of the warm ocean on the cold gap flow, we conducted four numerical experiments, namely Control, EP_1, EP_2 and EP_3 (Table 3), based on case B. Case B is a relatively moderate jet which has an air temperature of 267 K at the lowest model level and a sea surface temperature (SST) of 280 K in the LCI area. The control run employs the SST (280 K) from the RAMS data set and a full microphysics scheme considering the water substance as vapor, liquid and solid. This scheme is capable of producing clouds and precipitation. EP_1 uses the same microphysics scheme as the

control run but the SST is set to 267 K (in equilibrium with the atmospheric surface layer, eliminating an upward sensible heat flux). EP_2 treats all water substance as vapor (no hydrometeors are produced) and uses the SST same as the Control (280 K). EP_3 uses the same microphysics scheme as EP_2 and the SST is set to 267 K.

The simulation results show that SST has more impact on the flow than the moisture/cloud scheme. Runs with SST set to 267 K have stronger wind cores compared to the Control run Figure 11a, b, and c show the results from the Control run. (Here we will discuss differences among the sensitivity runs with respect to Figure 11.) EP_1 has a cooler marine layer (the 264 K isentrope reaches to 152.5W), a stronger jet core (30 ms^{-1}) but weaker surface winds (22 ms^{-1} in the core region). EP_2 has slightly cooler low level air just out side of the gap (the isentrope of 264 K reaches to 153.7W, figure not shown), the speed pattern does not change much. EP_3 has a cooler marine layer (the isentropic of 264 K reaches to 152W), stronger jet core (30 ms^{-1}) but weaker surface winds (22 ms^{-1} in the core).When the SST is set to the same as the surface air temperature, there is less turbulence transferring thermal energy from the sea surface to the jet and bringing kinetic energy from the jet to the surface layer. This results in a cooler marine layer and stronger jet core but weaker winds at the surface.

Table 3. SST and microphysics scheme choices of the numerical experiments.

Experiment	SST	Microphysics scheme
Control	RAMS data set	Vapor, liquid and solid
EP_1	267 K	Vapor, liquid and solid
EP_2	267 K	Vapor only
EP_3	RAMS data set	Vapor only

Figure 11. Vertical cross-section for the case on 26 November 2003. a) is along the latitude 59.3N, showing the potential temperature (K), horizontal wind speed and vertical motion (ms^{-1}) of the air; b) and c) are the potential temperature and horizontal wind speed along the jet core. The coast locates at 154W.

a)

vertical velocity (ms^{-1} shaded) wind speed (ms^{-1} broken lines) potential temperature (K solid lines)

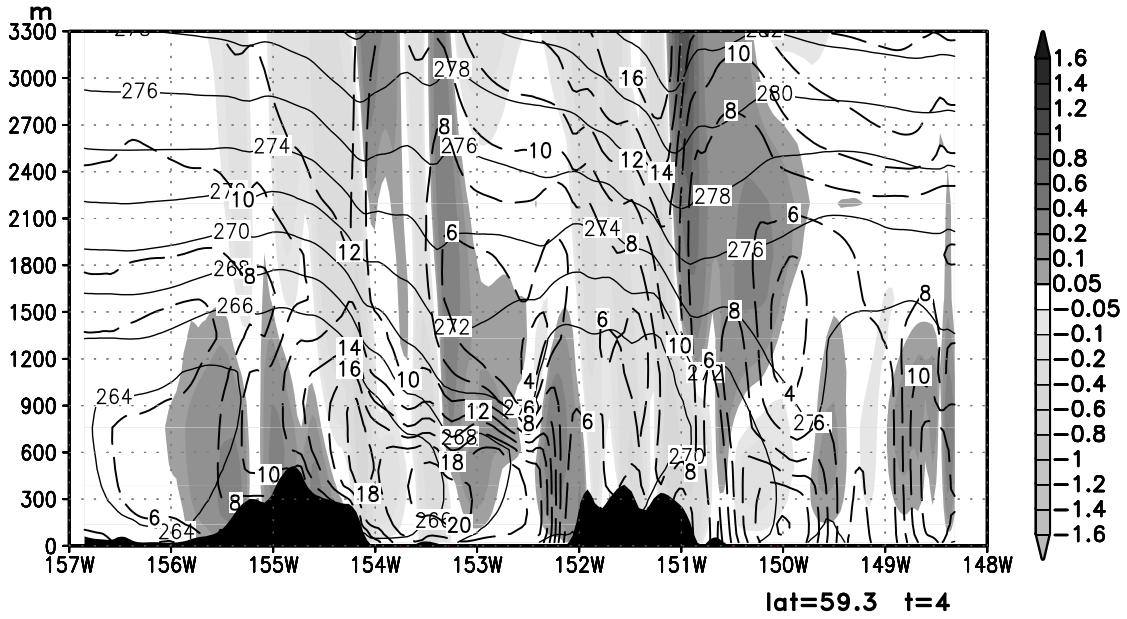

b)

potential temperature (K)

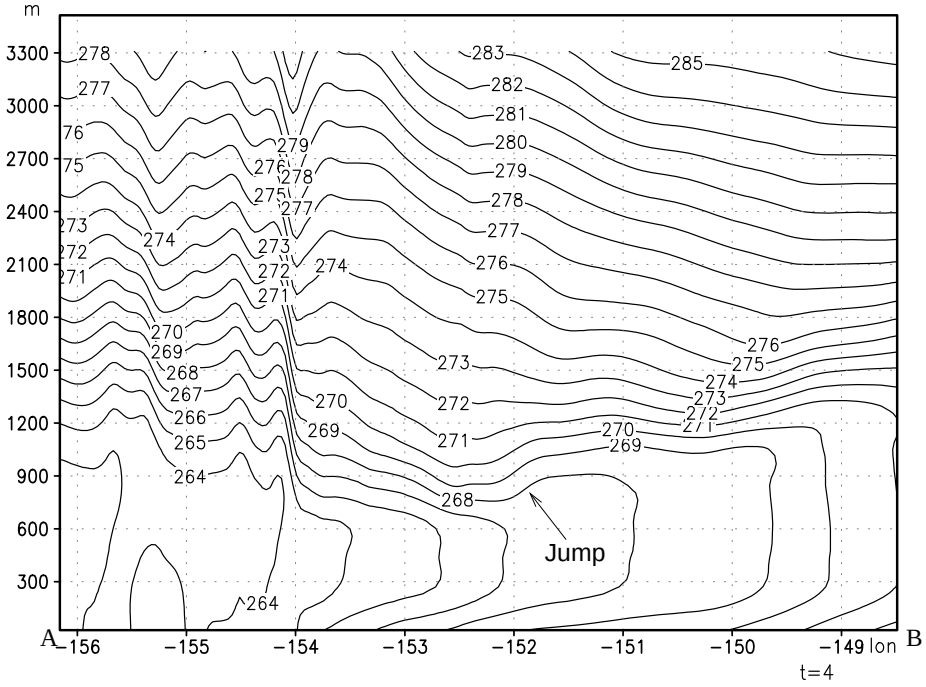

c)

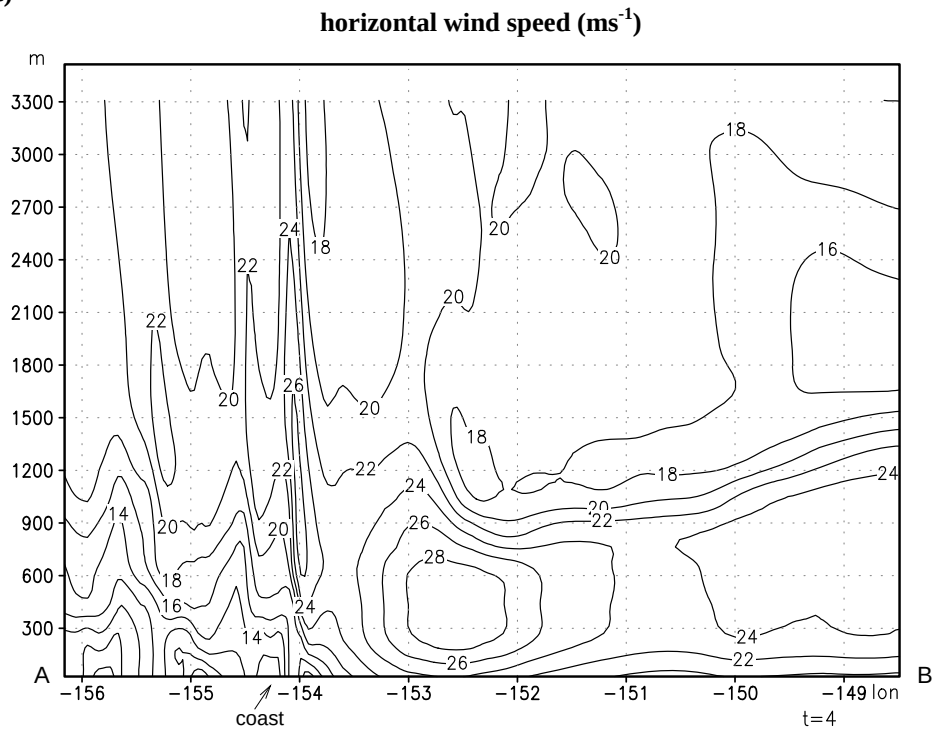

Influence of complex terrain

Comparing the simulations using the original topography and the simulations using simplified topography can reveal the influences of the complex terrain on air flows. To examine the influences of the complex terrain on gap flows in LCI, three sets of simulation were conducted, namely the control, S_1 and S_2 run. The simulation using the original topography is called control run. The simulation with the barriers in the ILA gap reduced to 1/100 of their original height is named S_1 run. This simplification leads to a smooth bed in the gap since the barriers in the ILA gap are lower than 600 m. Further simplifying the topography of S_1 run by cutting off the sidewall downstream of the gap generates the topography of the third simulation, S_2 run. The elevation contours in Figure 12 depict the simplifications of the topography of the lower Cook Inlet region for this study.

Figure 12. The grid 3 elevation plot of the lower Cook Inlet portion. The elevation contour interval is 100 m. a: the original topography; b: simplified topography for S_1 run; c: simplified topography for S_2 run.

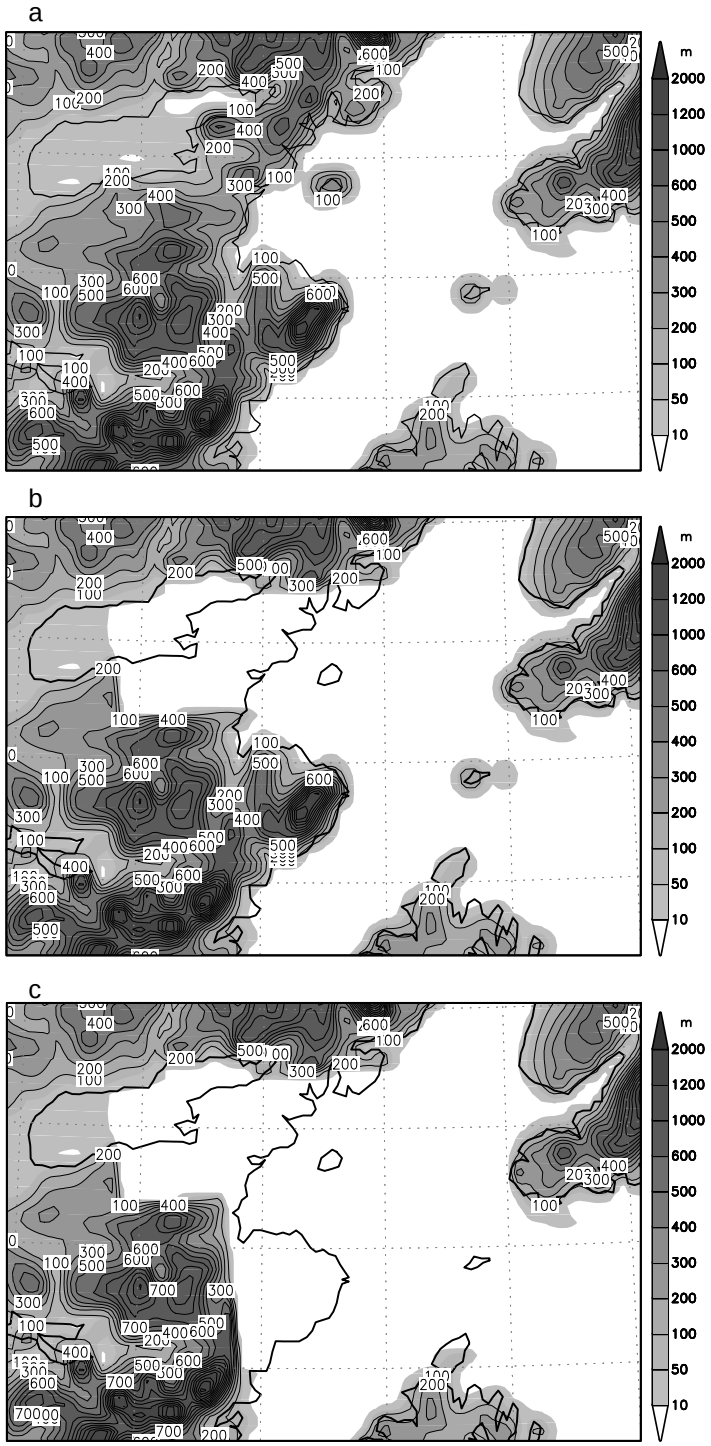

Barriers in the gap

Barriers in the gap block the flow in all three cases, no matter if the *Fr* of the incident flow is great than 1 (case B and C) or not (case A). The stronger jet core in the S_1 run than in the control run indicates that the barriers in the gap consume some energy of the incident flow in the gap either through friction, turbulence/wave generation or converting kinetic energy into potential energy which is then released at the lee side of the barriers. The flow accelerates rapidly in the gap exit zone also showing the blocking effect of the barriers.

The flow across the barriers has the typical characteristics of cross-barrier winds. Vertically propagating waves and oscillatory movement are all clear in these three cases. The blocking has little effect on the flow with high *Fr* and less stable incident flow. Case B shows less enhancing of the jet in the S_1 run then other two cases. Because case B has a less stable atmosphere and larger *Fr*, the air tends to flow over the barriers with little energy loss.

The barriers in the gap serve to reduce the decreasing rate of the planetary boundary layer height when the air flows from the land to the water. Case C demonstrates this clearly. The S_1 run case C has the northern part of the flow turning north-east into the Cook Inlet. Without the disturbance of barriers in the gap, the marine boundary layer (MBL) is so low that the Kenai Peninsula blocks the northern part of the flow and forces it to turn northeast into the Inlet.

Sidewall

The sidewall bounding the gap exit zone in the south serves as a constraint to the outflow. With this constraint, the outflow maintains a higher MBL and continues to accelerate down the stream of the sidewall. Without the sidewall, the outflow reaches its maximum speed earlier and the cores contrast to the coast. However, because of the lack of this continuing acceleration, the jet is not as strong as in the S_1 case. This is evident from the reduction of the areal extent of high wind in all three cases. The constraining effect of the sidewall to the flow is also noticeable from the change of the wind direction in the flow. The S_2 runs of case A and C both show that the wind direction turns a bit southward in the LCI. Without the constraint of the sidewall, the jet height is lowered. The contours of wind speed and/or potential temperature are approximately symmetric about the axis of the gap.

Jump in the jet flow

Low level air flowing with a high speed may experience a sudden decrease of speed and increase of the flow depth. This is referred to as a "hydraulic jump" (AMS 2000). The simulations show a jump just past the Barren Islands region while the MBL depth along the jet decreases away from the coast further into the ocean. Without the constraint of the sidewall, the outflow is spread across the flow and has a shallower MBL which leads to a weaker jump. Case A S_1 run has a jump from 360 m to 660 m east of 152W while the control is from 500 m to 600m. The S_2 jump is from 360 m to 540 m. Case B has a jump from 780 m to 1200 m in S_1 run. It is from 780 m to 1140 m in the control run and from 720 m to 1140 in the S_2 run. Case C does not show obvious jump but the boundary layer decreases from 540 m to 360 m in all three runs. Case C has a more stable upper level layer which caps the flow and prevents the vertical motion.

Flow Interaction in the lower Cook Inlet

Under certain circumstances, the down Cook Inlet jet (CId) and easterly jet in lower Cook Inlet (ILAr) occur at the same time and converge in lower Cook Inlet. This situation often rises when a low system traverses through the North Gulf of Alaska. Figure 13 Shows the Eta surface analysis at 00Z on 7 February, 17 February, and 24 February 2005, all periods in which CId and ILAr coexisted. They are typically characterized by a low pressure system or trough in the western Gulf of Alaska, easterly flows in the lower Cook Inlet, and down Inlet winds in the rest of Cook Inlet. The pressure in the Alaska interior is relatively higher than the coastal region such that the pressure gradients are directing channeled flows down Cook Inlet. The events on 7 February and 17 February have more intense pressure gradients over the east side of the Kenai Peninsula. The lower level easterly flows blocked by the coastal mountains tend to form a localized ridge parallel to the coast which induces a barrier jet.

Figure 14 gives SAR-derived and RAMS simulated wind for the above three events, depicting interacting CId and ILAr lower Cook Inlet. The SAR images were taken at about 03 UTC 7 February, 17 February, and 24 February 2005. The RAMS winds are those closest in time to the SAR images. (The color scale of the RAMS plots is the same as the SAR image.) The overall patterns of surface wind shown on SAR images and resolved by RAMS model are similar, though the model tends to somewhat under-predict wind speed. The northeasterly CId and easterly ILAr meet in lower Cook Inlet and create a narrow convergence zone which may cause strong turbulence (not resolved at these grid scales) and present a hazard to general aviation and marine traffic. The barrier jet induced by the blocking of the coastal mountains to the on-shore flow is apparent on the plots for both 7 February (Figure 14a) and 17 February (Figure 14b). The highest wind is just off the end of the barrier. The easterly flow of 24 February does not show barrier jet characteristics on RAMS simulation but rather more closely resembles a gap flow. The flow has a moderate speed (12 ms^{-1}) before entering the lower Cook Inlet and accelerates through the gap between the Kenai Peninsula and the Kodiak Island. Here we conclude that the easterly jet is likely the result of the channeling of the gap between the Kenai Peninsula and Kodiak Island of the strong easterly flow from the North Gulf of Alaska.

Figure 13. Eta surface analysis at 00Z on 7 February (a), 17 February (b) and 24 February (c) 2005. The magenta rectangle in c shows the geo-location of grid 3.

a)

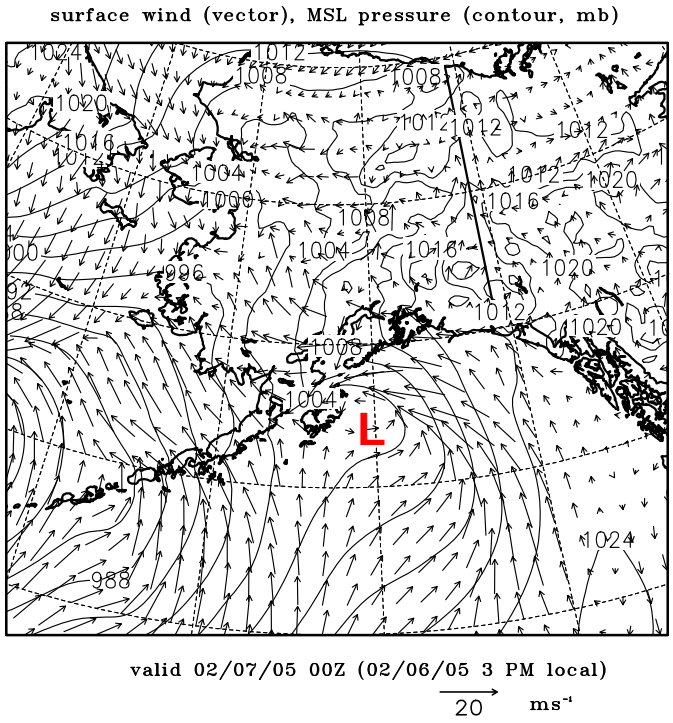

b)

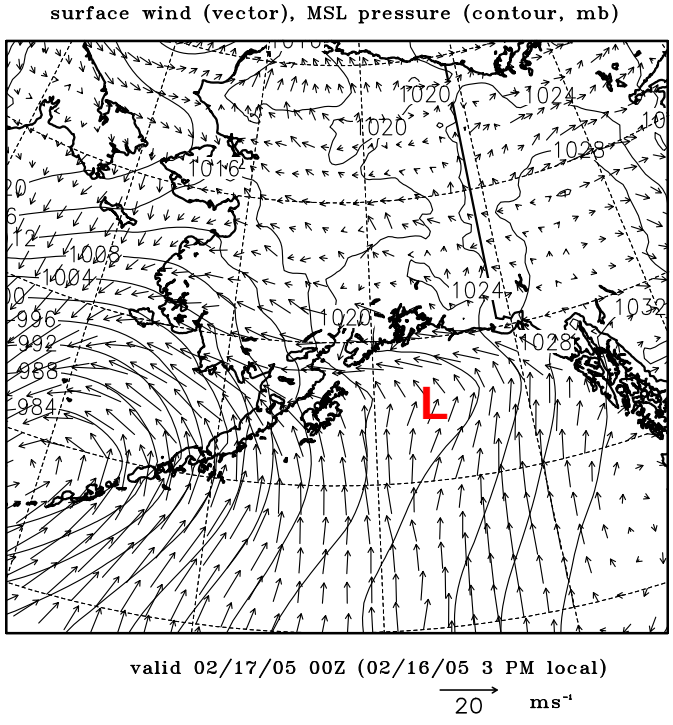

c)

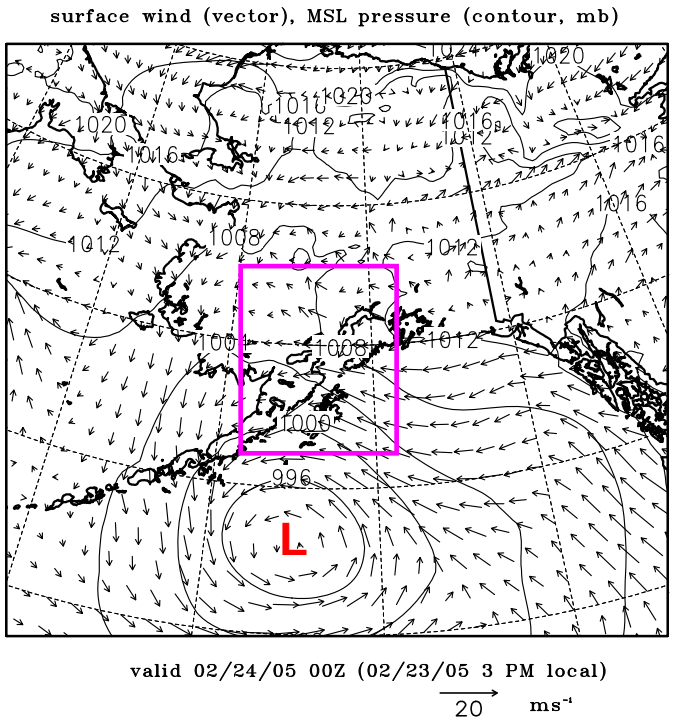
surface wind (vector), MSL pressure (contour, mb)
1020
1016
1012
1008
1004
1000
996
L
valid 02/24/05 00Z (02/23/05 3 PM local)
20 ms-1

Figure 14. SAR observation (left column) and RAMS simulation (right column) of strong down Inlet and easterly winds in the lower Cook Inlet. These SAR image were taken at about 03Z on 7 February, 17 February and 24 February 2005, corresponding RAMS winds are at 02Z.

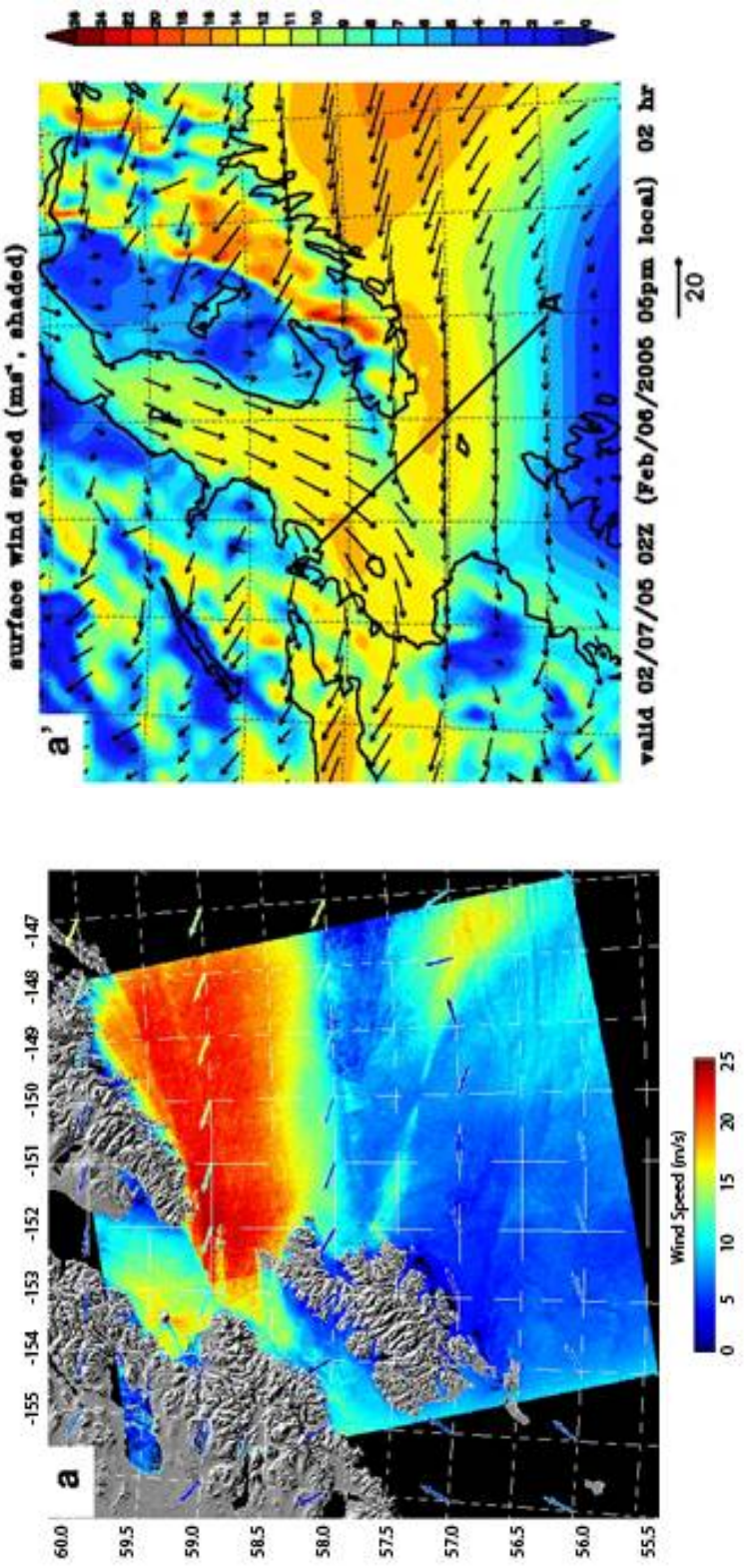

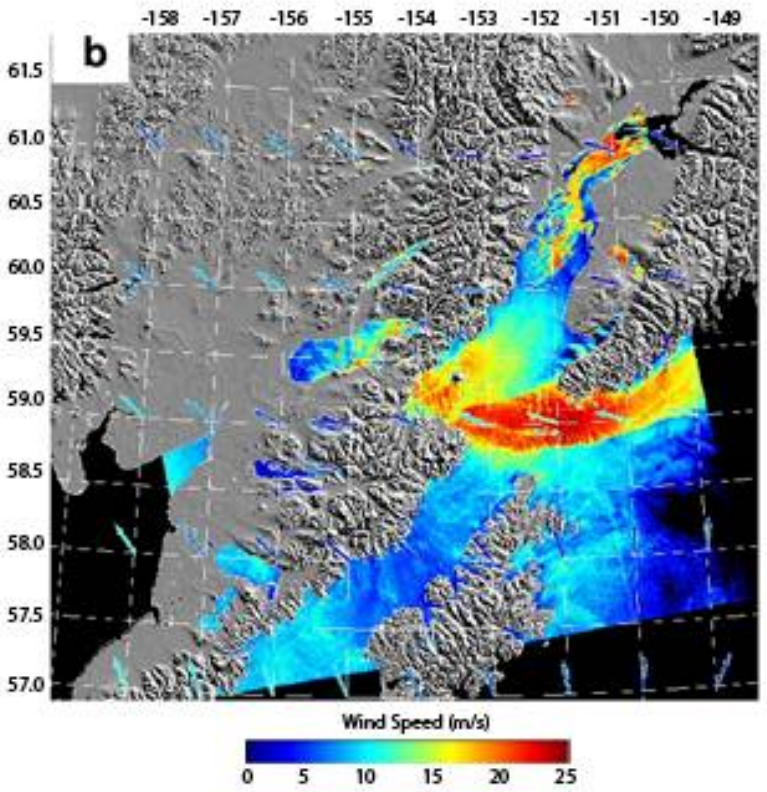
b
-158 -157 -156 -155 -154 -153 -152 -151 -150 -149
61.5
61.0
60.5
60.0
59.5
59.0
58.5
58.0
57.5
57.0
Wind Speed (m/s)
0 5 10 15 20 25

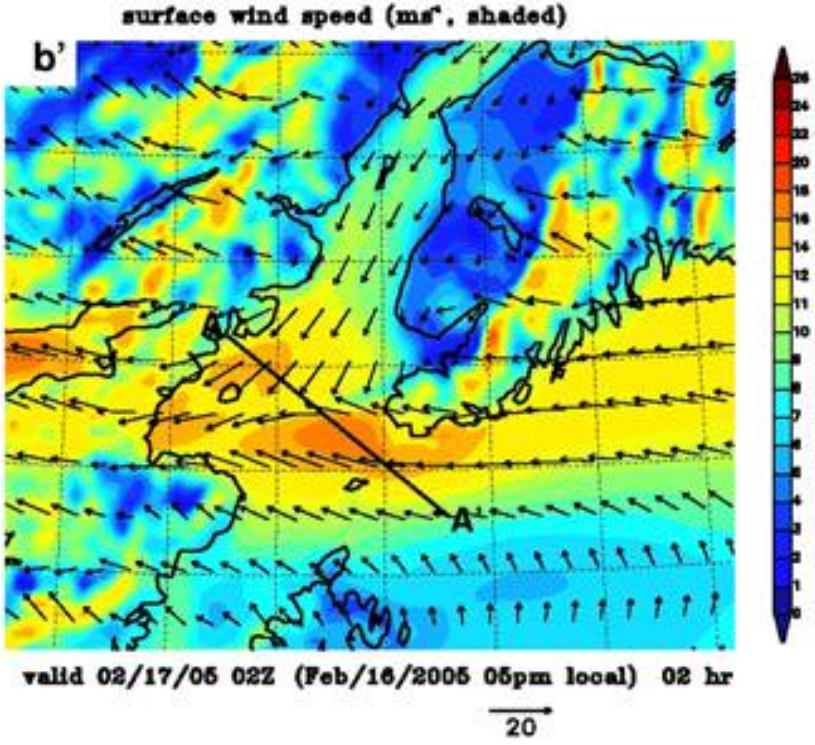
surface wind speed (ms', shaded)
b'
A
valid 02/17/05 02Z (Feb/16/2005 05pm local) 02 hr
20

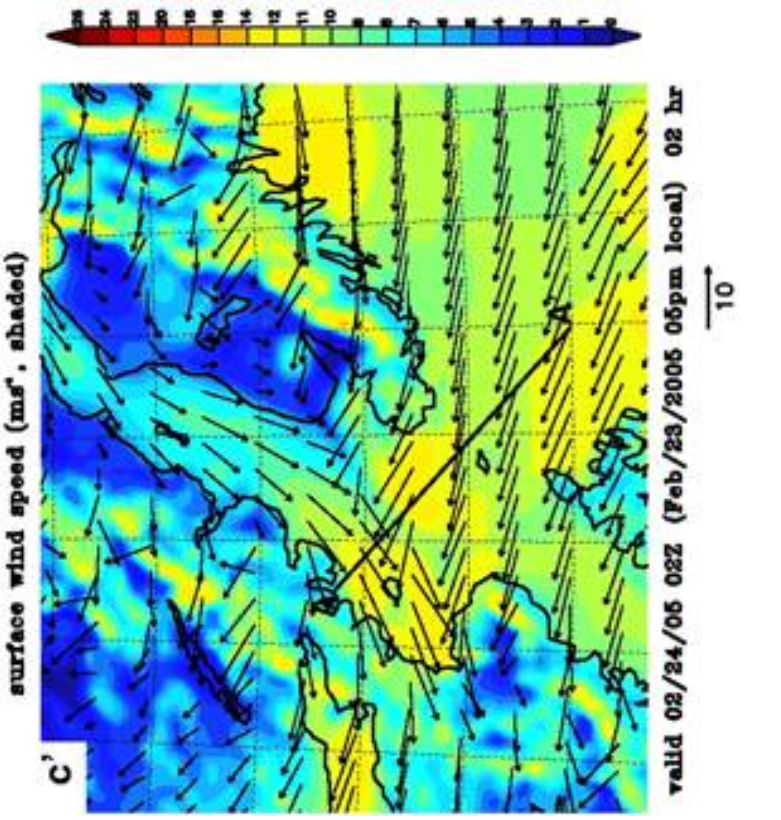
surface wind speed (ms", shaded)
c'
valid 02/24/05 022 (Feb/23/2005 05pm local) 02 hr
10

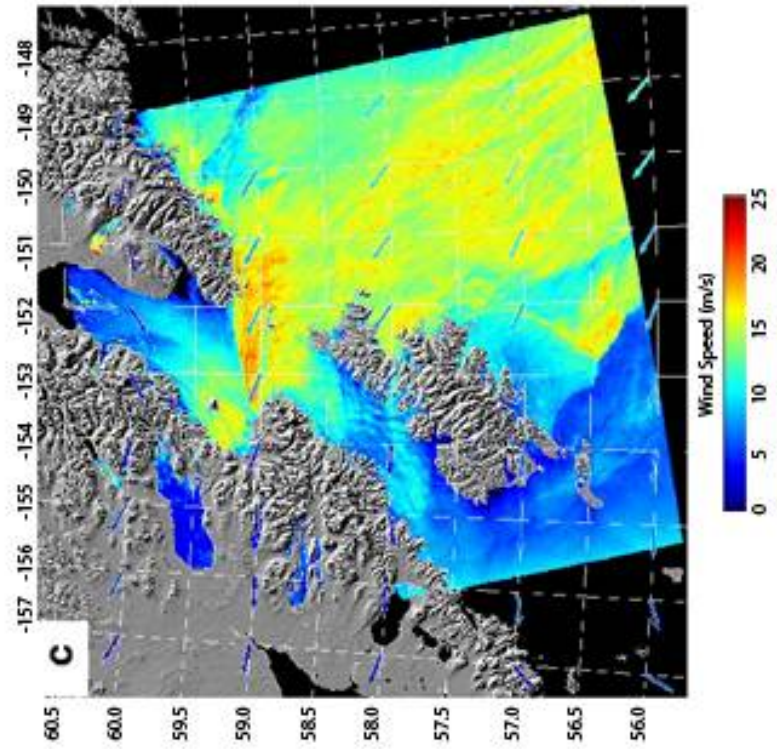
c
-157 -156 -155 -154 -153 -152 -151 -150 -149 -148
60.5 60.0 59.5 59.0 58.5 58.0 57.5 57.0 56.5 56.0
Wind Speed (m/s)
0 5 10 15 20 25

There are two automated surface observations (C-man stations) at the Augustine Island and the Barren Islands respectively. Table 4 and 5 show the surface wind observations at these two locations, Augustine Island and Barren Islands (Figure 3). Note the SAR-wind speed is estimated from the SAR-wind image so only a possible range is given. There are some differences between the C-man observations, RAMS wind and SAR wind. It seems there is more agreement at Augustine Island. Overall, the direction differences are within 30 deg which is within the error range of 45 deg of onshore and offshore observation (Hsu, 1998). Note that the simulations seem to under-predict wind speed at these locations.

Table 4. Wind at Barren Islands at 03Z on 7 February, 17 February, and 24 February 2005.

Date	C-man		RAMS		SAR
	WSPD (ms^{-1})	WD (deg)	WSPD (ms^{-1})	WD (deg)	WSPD (ms^{-1})
07/Feb/05	17.5	64	12.4	93	24-25
17/Feb/05	17.0	67	12.8	103	22-23
24/Feb/05	9.7	95	10.3	105	15-16

Table 5. As Table 4 but Augustine Island.

Date	C-man		RAMS		SAR
	WSPD (ms^{-1})	WD (deg)	WSPD (ms^{-1})	WD (deg)	WSPD (ms^{-1})
07/Feb/05	14.4	49	12.6	71	14-15
17/Feb/05	13.3	48	13.5	61	15-16
24/Feb/05	11.8	54	10.8	69	12-13

Figure 15 gives the cross-section of these three events at lines AA' in Figure 14. The location is chosen such that the cross section is normal to the convergence zone between CId and ILAr. Figure 15a gives a view of flows on 7 February 2005 from the surface to the height of more than 2000 m. The surface convergence line is at about 152.5W, above which the upward vertical velocity is vigorous. The flows have the same direction above 500 m which indicates the depth of CId. Similarly, Figure 15b is for 17 February 2005. The surface convergence line is at 152.7W, the depth of CId is about 400 m. The high resolution simulation (1 km grid spacing) will show more details in the next section. Figure 15c is for 24 February 2005. This is a weak event, the depth of CId is less than 200 m height. The surface convergence line is at 152.7W.

Figure 15. Vertical cross-section for 07 February (a), 17 February (b), and 24 February (c) 2005. The location is shown on Figure 14 by lines AA'. The solid lines are isentropes, the dotted line is wind (ms^{-1}); the shades is the vertical velocity (ms^{-1}).

a)

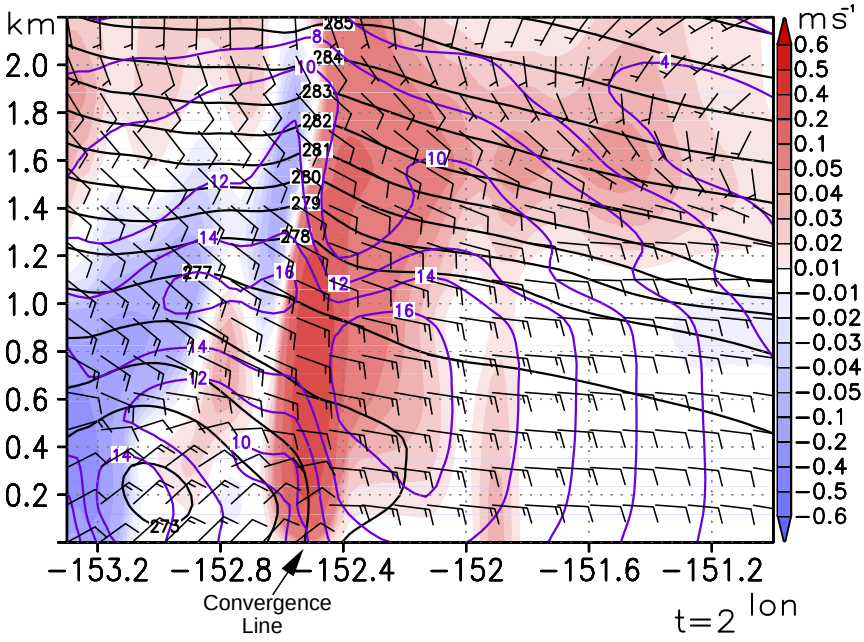

b)

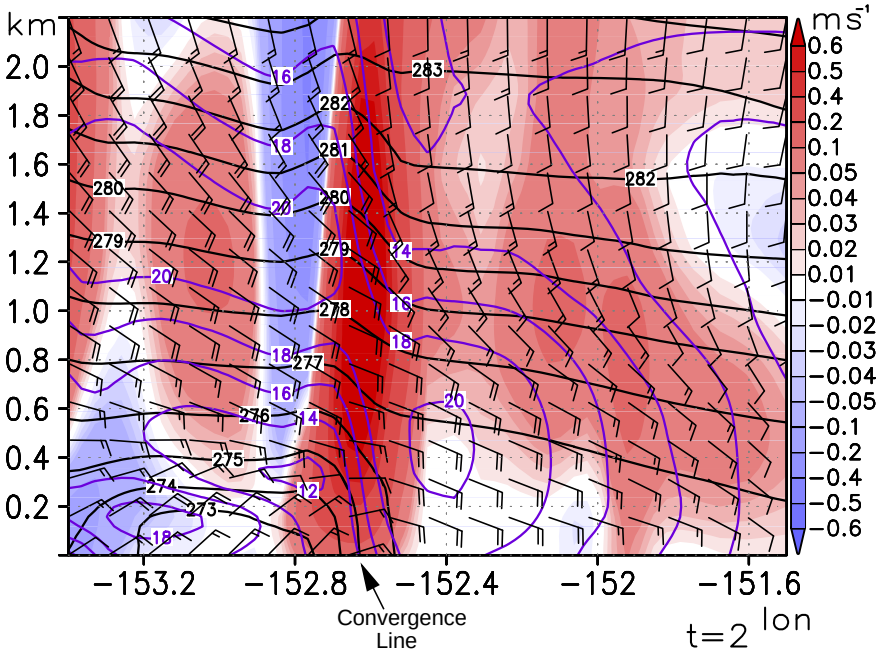

c)

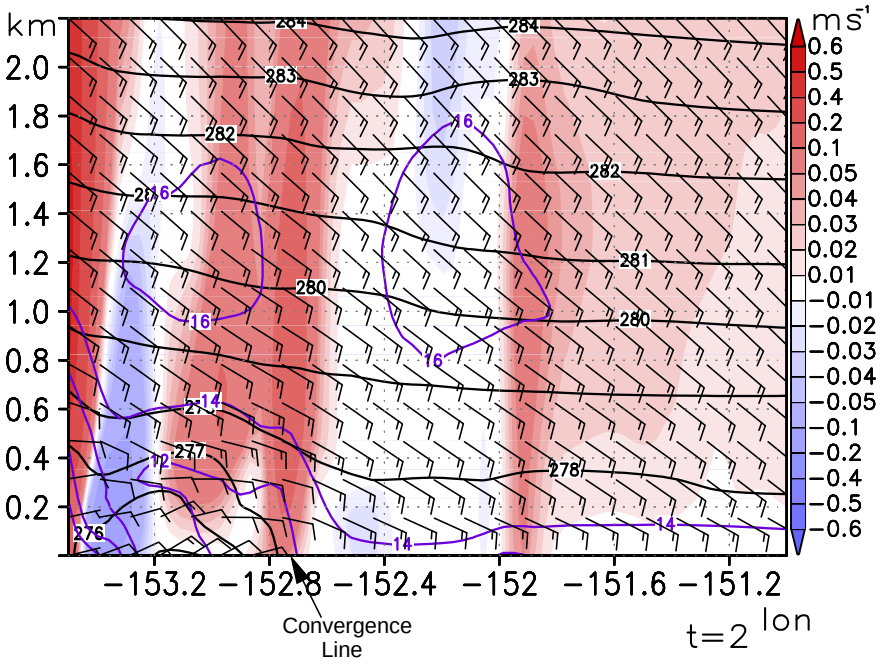

Very high-resolution simulation

Figure 15 shows some characteristics of the surface front: zero-order discontinuities in density (temperature) and wind velocity (Shapiro and Keyser 1990) in the convergence zone for all three cases. However, the fine structure along the convergence zone is dim, e.g. the vertical velocity is less than 0.8 ms^{-1}. From the plot of observed cases (Shapiro and Keyser 1990), the scale of these fine structures is on the order of a few hundred meters to 1 km. Therefore, we conducted a very high-resolution (1km grid spacing) simulation for the case of 17 February 2005. The fourth nested grid of 202 by 202 points covering the whole lower Cook Inlet region was included in addition to the previous three nested grids. The plots from the model output are shown on Figure 16.

Figure 16a is the two dimensional plot of the horizontal wind speed, temperature and sea level pressure. A very narrow zone of about 3 km width formed between CId and ILAr in lower Cook Inlet. The CId side is 2° warmer than the ILAr side. Compared to the 4 km simulation (Figure 14b'), the winds are stronger in the 1 km simulation in that the areas with high speed are larger, the edge of convergence zone is sharper, more closely resembling the SAR-wind image. Figure 16b shows the near "zero-order" discontinuities in density and wind velocity between air masses from CId and ILAr. It also shows the vertical velocity as high as 2.3 ms^{-1} at the convergence zone. The significant vertical movement reaches as high as 1800 m above the sea surface. It is clearly a hazard to the aviation traffic in this region.

Figure 16. The very-high-resolution simulation of the case on 17 February 2005. a: the horizontal plot of surface wind (shaded), temperature and sea level pressure; b: the cross-section along the same line for Figure 14b.

a)

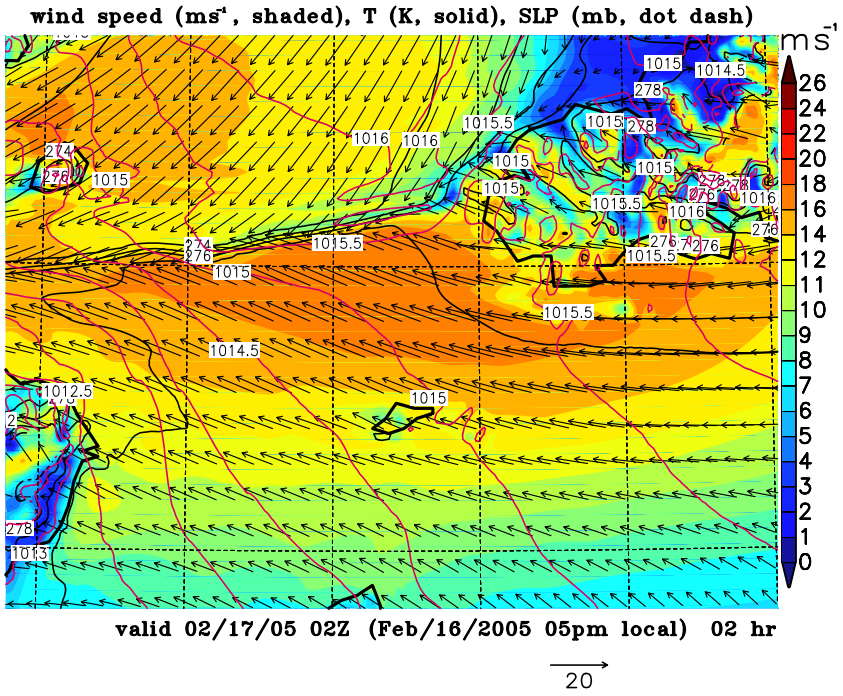

b)

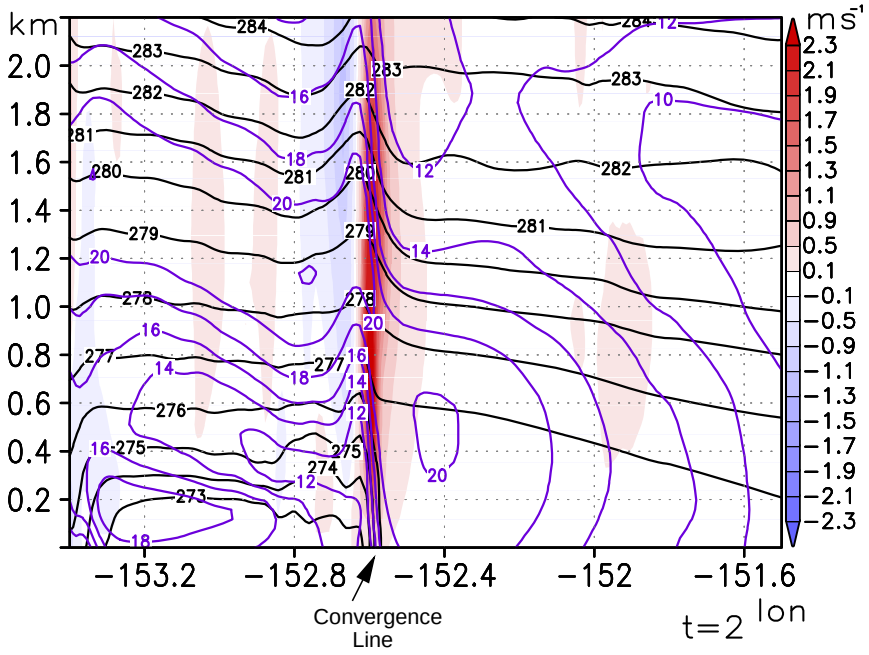

Winds in the Shelikof Strait

Winds in Shelikof Strait can be mainly divided into 4 categories: up-Strait (SKFu), down-Strait (SKFd), cross the Strait westerly (KYG and PB) and cross the Strait easterly. The down-Strait winds are dominant (Liu, et. al. 2006). As frequent synoptic high/low pressure systems traverse through the Gulf of Alaska, there are frequently strong pressure gradients along the Shelikof Strait and according to Bond and Stabeno, (1998) the wind should blow down the pressure gradients *along* the Strait. However, this is not necessary true in our findings. There are cases of cross-Strait winds and along-Strait winds under similar along-strait pressure gradients. Whether the flow runs across the Strait or up/down along the Strait is not solely determined by the pressure gradients, the characteristics of the incident airmass also play an important part.

The reason that there are more down-Strait than up-Strait gap winds is partially that the west boundary of the Strait is much higher than the east boundary. Figure 17 shows the schematics of flow in Shelikof Strait with pressure gradients along the Strait. To have up-Strait gap winds, there must be strong pressure gradient force pointing up-Strait. This can occur when the center of a low system is located to the north of the Strait or a high system is located to the south of the Strait. In either situation the background flow will be from the west to the east. When the flow is not stable enough that Froude number is greater than 1, the airmass will flow across the high west boundary and the low east boundary. Therefore, there is no up-Strait gap wind. When the air is well stratified and stable enough to have a Froude number less than 1, the flow is blocked by the west boundary. The airmass will flow eastwards through some gaps with lower elevation in the west boundary. There is no up-Strait gap wind either. This is also the reason that there are many cross-Strait gap events at gaps such as Kaguyak and Puale Bay (Liu, et al. 2006) in the Strait.

Figure 17. Schematics showing flows under along strait pressure gredients. H indicates high pressure, L low pressure.

a)

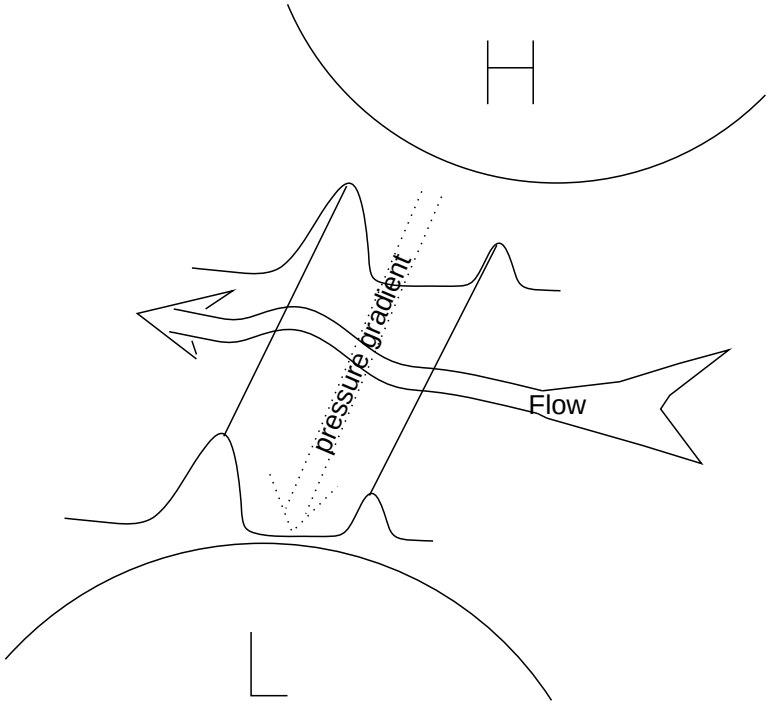

b)

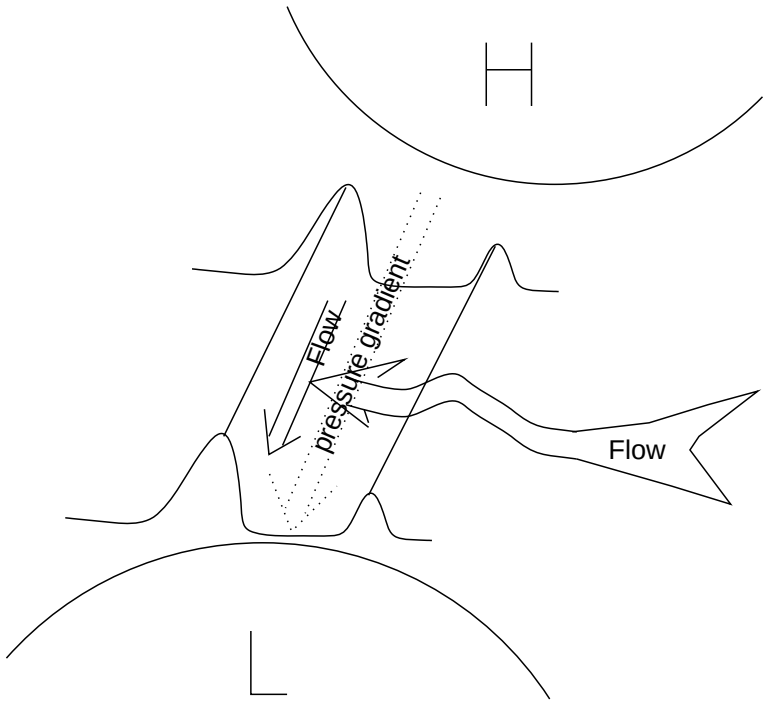

c)

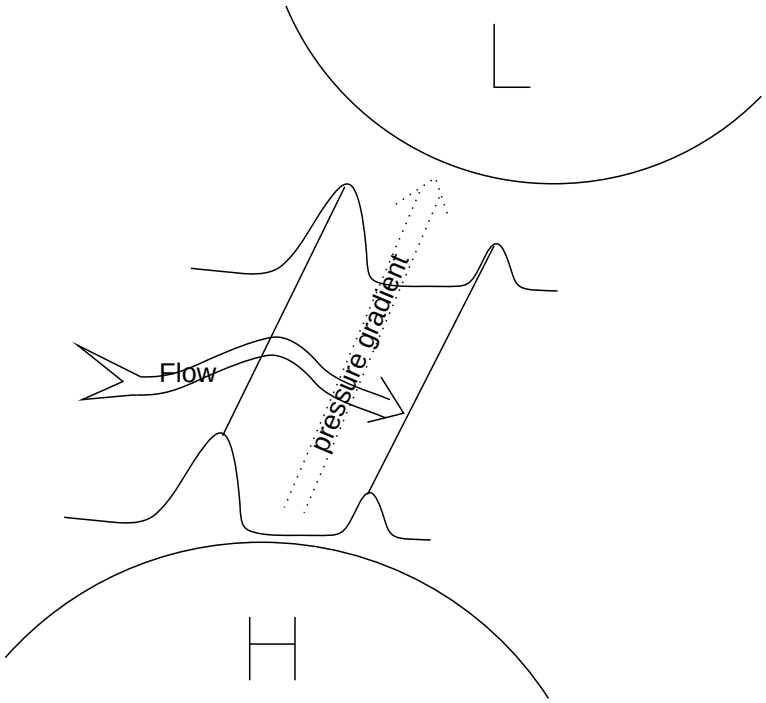
L
pressure gradient
Flow
H

d)

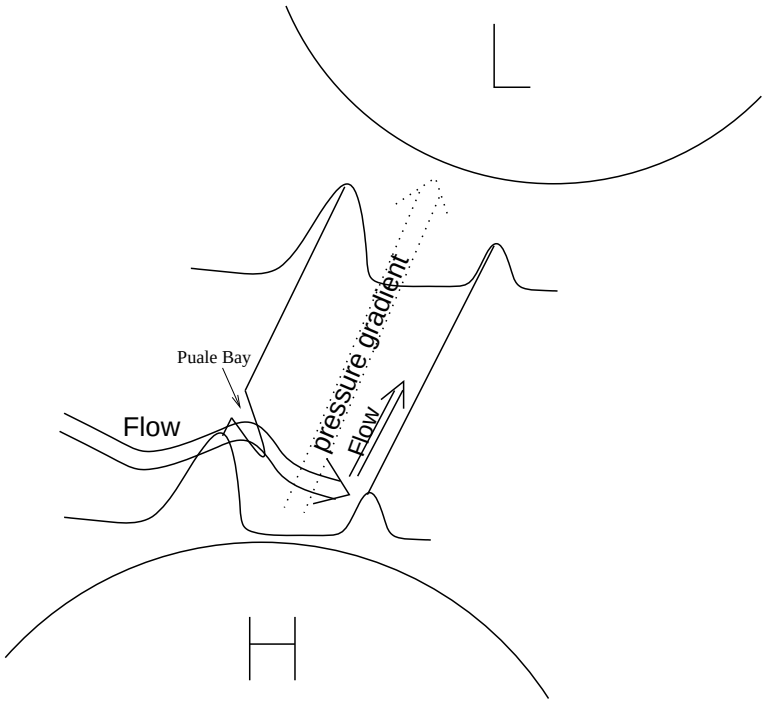
L
pressure gradient
Puale Bay
Flow
Flow
H

CONCLUSIONS

The capability of high resolution numerical mesoscale modeling was established at AEFF. The modeling system was employed to characterize the low-level wind jets in the Cook Inlet and Shelikof Strait, Alaska. There were 10 different major regimes classified as a function of location and direction. These jets were further grouped into four more general categories: the cross-channel westerly and easterly, and the up (south-westerly) and down (north-easterly) channel jets. The relative locations and intensities of the transient low and high pressure systems determine the occurrence, strength and duration of a jet.

With frequently occurring favorable synoptic-scale pressure configurations, some form of low-level jet occurred nearly every day in this region. The most frequently occurring jet was the ILA which presented almost one third of the period. The low-level wind jets were highly associated with recognizable large-scale pressure systems in this region. Strong pressure gradients along the gap are responsible for the cross-channel jets while the jets along the Inlet can result from either strong pressure gradients along the Inlet or by the channeling of the along-Inlet synoptic scale flows.

As an independent source, the SAR-derived winds were compared with the RAMS forecasts. The comparison between SAR-derived wind and RAMS wind showed the capability of RAMS to simulate the low-level wind jets in Cook Inlet and Shelikof Strait for those cases. The RAMS output can be used to give the forecaster and ordinary user valuable direct guidance for forecasting strong low-level winds in Cook Inlet and Shelikof Strait. We believe that the climatology of wind events and their associated synoptic pressure patterns can act as further guidance in forecasting surface wind jets from the coarser-grid NCEP model forecasts.

The Iliamna Jet is shaped by the surrounding topography, the incoming air and the ocean. Because the Iliamna Gap is a coastal gap which has an unlevel bed, and is surrounded by complex terrain and oceans, the Iliamna Jet has its own special characteristics. Three gap wind events with various incident flow of different Froude Number were simulated using high resolution mesoscale model to characterize the Iliamna jet in the lower Cook Inlet Alaska. The 4 km grid spacing simulations revealed interesting structures of the gap wind: a small scale high wind zone above the seaward edge of the gap, a vertically propagating wave above this limited high wind zone, followed by a transition zone in which the wind speed increases, then a high speed core. The model simulation and the SAR observation show that the jet can extend eastwards several hundred kilometers from the coast which is much longer in distance than documented by Macklin et al. (1990).

The unlevel bed of the gap induced a mountain wave-like feature (the small high speed zone and the vertically propagating wave). The uneven terrain at the seaward end of the gap causes more air to flow out through the lower part of the gap and the jet core is located more along the south side of the LCI. The side wall down stream of the gap prevents the jet from turning right. The warm ocean actually slows down the jet via the upward moisture and downward kinetic energy exchange. The stability of the atmosphere

greatly affects the distance the vertical propagating wave can travel. The more stable the atmosphere, the less distance the wave can travel. The stability of upper tropospheric layers also influences the strength of the jet. The more stable the upper level atmosphere, the stronger the jet.

The sidewall downstream of the gap serves as a constraint to the out flow. With this constraint, the outflow maintains a higher MBL and continues to accelerate down the stream of the sidewall. Without the sidewall, the out flow reaches its maximum speed early, the core is closer to the coast and the jet is weaker. The constraining effect of the sidewall to the flow is also noticeable from the change of the wind direction in the flow. Without the constraint of the sidewall, the jet height is lowered. The contours of wind speed and/or potential temperature are approximately symmetric about the axis of the gap. There is a jump just pass the Barren Islands region while the boundary layer depth along the jet decreases away from the coast further into the ocean. Without the constraint of the sidewall, the outflow is spread across the flow and has a shallower boundary layer which leads to a weaker jump.

A gap flow is expected to have a fan-like turning which is driven by the Coriolis force and is positively proportional to the flow speed and the latitude (Steenburgh, et al. 1998). ILA jets often occur when there is a low in the north Gulf of Alaska and a high in the west of Alaska, which forms a strong pressure gradient along the ILA gap. However, the low is usually located north to the LCI and there is a strong pressure gradient pointing north ward and balancing the Coriolis force imposed on the outflow preventing the fan-like turning in an ILA jet.

The North Gulf of Alaska is a wind-prone area. Low pressure systems traversing through the Gulf induce strong winds in the coastal region. Frequently, the strong down-Inlet wind converges with the strong easterly wind in the lower Cook Inlet and creates strong vertical velocities and associated turbulence up to 2000 m height which is a hazard to the local aviation. The southerly down-Inlet jet is a down-gradient flow resulting from the confining terrain bounding Cook Inlet on both sides. The strong easterly wind is in some cases a barrier jet caused by the blocking of the Kenai Peninsula to the easterly flow from the Gulf and in others a gap wind crossing the gap between the Kenai Peninsula and the Kodiak Island. The depth of these down-Inlet jets is less than 500 m. Therefore the interaction zone is shallow. The 4 km resolution RAMS winds show similar horizontal structure as the SAR-derived wind while the 1 km very high-resolution simulation showed more agreement with SAR-imagery.

Whether the flow runs across the Shelikof Strait or up/down along the strait is not solely determined by the pressure gradients, the characteristics of the airmass also play an important part. The fact that the west boundary of the Strait is much higher than the east boundary plays a main role in inducing more down-Strait than up-Strait gap wind.

This project provided the opportunity to study the near surface weather in Cook Inlet and Shelikof Strait. Due to time limitations, we focused on the strong surface winds that have significant impact on the local aviation and marine activities. Other severe weather such

as snow storms and heavy rainfall also profoundly affect the daily lives of the people in this region. Finally, how will the changing climate affect weather in Cook Inlet and Shelikof Strait? We feel compelled to address these questions as well, if the opportunity presents itself.

ACKNOWLEDGEMENT

This work was funded by Minerals Management Service through the University of Alaska Coastal Marine Institute and by matching funds from the University of Alaska Anchorage Aviation Safety Initiative. The authors would like to thank NOAA/NCEP for the use of Eta data, and Johns Hopkins University/Applied Physics Laboratory for the use of SAR images.

STUDY PRODUCTS

Archive of data and graphics of three years of high-resolution numerical simulations of 3D weather conditions of Cook Inlet and Shelikof Strait of Alaska.

Archive of SAR-images over Cook Inlet and Shelikof Strait.

Liu, H., P.Q. Olsson, K. Volz, H. Yi. 2006. A Climatology of Mesoscale Model Simulated Low-Level Wind Jets Over Cook Inlet and Shelikof Strait, Alaska, Estuarine, Coastal and Shelf Science, 70, 551-566.

Liu, H., P.Q. Olsson. 2006. The Westerly Gap Wind in Lower Cook Inlet, Alaska (I)—Observation and Simulation. Submitted to Monthly Weather Review.

Liu, H., P.Q. Olsson, K. Volz, H. Yi. 2006. The Westerly Gap Wind in Lower Cook Inlet, Alaska (II)—Sensitivity to Topography. *Manuscript in progress*.

Liu, H., P.Q. Olsson, K. Volz, H. Yi. 2006. Winds in the Shelikof Strait: Down Strait or Cross the Strait?. *Manuscript in progress*.

Liu, H., P.Q. Olsson, K. Volz, H. Yi. 2004. A Climatology of Mesoscale Model Simulated Low-Level Wind Jets Over Cook Inlet and Shelikof Strait, Alaska. The Seventh International Marine Environmental Modeling Seminar, Washington D.C., USA, Oct 19-21, 2004.

Liu, H., P.Q. Olsson, K. Volz, H. Yi. 2005. A Climatology of Mesoscale Model Simulated Low-Level Wind Jets Over Cook Inlet and Shelikof Strait, Alaska. University of Alaska Coastal Marine Institute Annual Research Review, March 8 2005.

Liu, H., P.Q. Olsson, K. Volz, H. Yi. 2006. RAMS simulated and SAR observed Flow Interactions in the Lower Cook Inlet, Alaska. The 14th Conference on Satellite Meteorology and Oceanography, 29 January – 2 February 2006, Atlanta, Georgia, USA.

Liu, H., P.Q. Olsson, K. Volz, H. Yi, 2006. RAMS simulated and SAR observed Flow Interactions in the Lower Cook Inlet, Alaska. University of Alaska Coastal Marine Institute Annual Research Review, 14, February 2006.

Olsson, P. Q. Cook Inlet Atmospheric Model. "Presented at: Cook Inlet Physical Oceanography Workshop Homer, AK: Alaska Ocean Observing System; Cook Inlet Regional Citizens Advisory Council; Kachemak Bay Research Reserve, 2005.

Olsson, P.Q. "High-Resolution Numerical Modeling of Near-Surface Weather Conditions Over Alaska's Cook Inlet and Shelikof Strait [Abstract]." Annual Report No. 10, University of Alaska Coastal Marine Institute. OCS Study MMS 2004-002. University of Alaska, Coastal Marine Institute and USDOI, MMS, Alaska OCS Region, Fairbanks, AK, 2004.

Olsson, P.Q. "High-Resolution Numerical Modeling of Near-Surface Weather Conditions Over Alaska's Cook Inlet and Shelikof Strait." Annual Report No.11, University of Alaska Coastal Marine Institute. OCS Study MMS 2005-055. University of Alaska, Coastal Marine Institute and USDOI, MMS, Alaska OCS Region, Fairbanks, AK, 2005.

Olsson, P.Q. "High-Resolution Numerical Modeling of Near-Surface Weather Conditions Over Cook Inlet and Shelikof Strait." Proceedings of the Tenth MMS Information Transfer Meeting and Barrow Information Update Meeting, pp. 16-17Anchorage, AK: Prepared by MBC Applied Environmental Sciences, Costa Mesa, CA for MMS Alaska OCS Region, 2005.

REFERENCES

AMS, Glossary of Meteorology. 2000. http://amsglossary.allenpress.com/glossary.

Arritt, R.W., T.D. Rink, Segal, D.P. Todey, C.A. Clark, M.J. Mitchell, and K.M Labas. 1997. The great plains low-level jet during the warm season of 1993. Monthly Weather Review 125, 2176-2192.

Blackadar, A.K. 1957. Boundary layer wind maxima and their significance for the growth of nocturnal inversions. Bulletin of American Meteorological Society 38, 283-290.

Bond, N.A., S.A. Macklin. 1993. Aircraft observations of offshore-directed flow near Wide Bay, Alaska. Monthly Weather Review 121, 150-161.

Bond, N.A., P.J. Stabeno. 1998. Analysis of surface winds in Shelikof Strait, Alaska, using moored buoy observations. Weather and Forecasting 13, 547-559.

Boner, W.D. 1968. Climatology of the low-level jet. Monthly Weather Review 96, 283-290.

Buckley, R.L., A.H. Weber, J.H. Weber. 2002. Statistical comparison of forecast meteorology with observations using the Regional Atmospheric Model System. 16th Conference on probability and statistics in the Atmospheric Sciences, 13-17 January 2002, Orlando, Florida, American Meteorological Society.

Cohn, S. A. 2004. Flow in complex terrain: observations by Radar Wind Profile and anemometers near Juneau, Alaska. Journal of Applied Meteorology 43, 437-448.

Coleman, B.R., C.F. Dierking. 1992. The Taku wind of Southeast Alaska: its identification and prediction. Weather Forecasting 7, 49-64.

Colle, B.A., C.F. Mass. 1996. An observational and modeling study of the interaction of low-level southwesterly flow with the Olympic Mountains during COAST IOP 4. Monthly Weather Review 124, 2152-2175.

Colle, B.A., C.F. Mass. 2000. High-Resolution observations and numerical simulations of easterly gap flow through the Strait of Juan de Fuca on 9-10 December 1995. Monthly Weather Review 128, 2398-2422.

Copeland, J.H., R.A. Pielke, T. Kittel. 1996. Potential climatic impacts of vegetation change: a regional modeling study. Journal of Geophysical Research (D) 101, 7409-7418.

Cotton, W.R., R.A. Pielk, R.L. Walk, G.E. Liston, C.J. Tremback, H. Jiang, R.L. McAnelly, J.Y. Harrington, M.E. Nichols. 2003. RAMS 2001: Current and future directions. Meteorology and Atmospheric Physics 82, 5-29.

Cotton, W.R., G. Thompson, P.W. Mielke. 1994. Real-time mesoscale prediction on workstations. Bulletin of American Meteorological Society 75, 349-362.

Doran, J.C., S. Zhang. 2000. Thermally driven gap winds into the Mexico City basin. Journal Applied Meteorology 39, 1330-1340.

Dorman, C.E., R.C. Beardsley, R. Limeburner. 1995. Winds in the Strait of Gibraltar. Quarterly Journal of the Royal Meteorological Society 121, 1903-1921.

Glickman, Todd S. 1999. Glossary of Meteorology. American Meteorological Society, http://amsglossary.allenpress.com/glossary

Harrington, J.Y., T. Reisin, W.R. Cotton, S.M. Kreidenweis. 1999. Exploratory cloud resolving simulations of arctic stratus. Part II: Transition-season clouds. Atmospheric Research 51, 45-75.

Hsu, S.A., 1988. Coastal Meteorology. Academic Press, Inc. San Diego, pp 260.

Jackson, P.L., D.G. Steyn. 1994. Gap winds in a Fjord Part I: observation and numerical simulation. Monthly Weather Review 122, 2645-2665.

Liu, H., P.Q. Olsson, K. Volz, H. Yi. 2006. A Climatology of Mesoscale Model Simulated Low-Level Wind Jets Over Cook Inlet and Shelikof Strait, Alaska. Estuarine, Coastal and Shelf Science, in press.

Lackman, G.M., J.E. Overland. 1989. Atmospheric structure and momentum balance during a gap-wind event in Shelikof Strait, Alaska. Monthly Weather Review 117, 1817-1833.

Liston, G.E., R.A. Pielke. 2000. A climate version of the regional atmospheric modeling system. Theoretical and Applied Climatology 66, 29-47.

Macklin, S.A., N.A. Bond, J.P. Walker. 1990. Structure of a Low-Level jet over Cook Inlet, Alaska. Monthly Weather Review 118, 2568-2578.

Macklin, S.A., J.E. Overland, J.P. Walker. 1984. Low-level gap winds in Shelikof Strait. Third Conference on Meteorology of coastal zone. Jan 9-13, 1984, Maimi, Florida, American Meteorological Society.

Macklin, S.A., R.W. Lindsay, R.M. Reynolds. 1980. Observations mesoscale winds in an orographically dominated estuary: Cook Inlet, Alaska. Proceedings of second conference on coastal meteorology, Jan 30-Feb 1, 1980. Los Angeles, American Meteorological Society.

Macklin, S.A., G.M. Lackman, J. Gray. 1988. Offshore-directed winds in the vicinity of Prince William Sound, Alaska. Monthly Weather Review 116, 1289-1301.

Marty, B., M. Weissbluth, R. Walko. 2000. Definitions and issues with RAMS topography and the vertical grid structure. 4th RAMS Users Workshop - 22-24 May, 2000, Cook College - Rutgers University, New Jersey, USA.

Malcher J., H. Kraus. 1983. Low-Level Jet phenomena described by an integrated dynamical PBL model. Boundary-Layer Meteorology 27, 327-343.

Mass, C.F., S. Businger, M.D. Albright, Z.D. Tucker. 1995. A windstorm in the lee of a gap in a coastal mountain barrier. Monthly Weather Review 123, 315-331.

Monaldo, F. 2000. The Alaska SAR demonstration and near-real-time synthetic aperture radar winds. Johns Hopkins Applied Physics Lab Tech. Digest 21, 49-57.

Olsson, P.Q., W.R. Cotton. 1997a. Balanced and unbalanced circulations in a primitive equation simulation of a midlatitude MCC. Part 1: The numerical simulation. Journal of the Atmospheric Sciences, 54, 457-478.

Olsson, P.Q., W.R. Cotton. 1997b. Balanced and unbalanced circulations in a primitive equation simulation of a midlatitude MCC. Part 2: Diagnosis of the balanced components. Journal of the Atmospheric Sciences, 54, 479-497.

Olsson, P.Q., J.Y. Harrington, G. Feingold, W.R. Cotton, S.M. Kreidenweis. 1998. Exploratory cloud-resolving simulations of boundary layer Arctic stratus clouds. Part I; Warm-season clouds. Atmospheric Research 47-48, 573-597.

Olsson, P.Q., J.Y. Harrington. 1999. Rapid frontogenesis and low-level jet formation along an ice coastline. Third Conference on Coastal Atmospheric and Oceanic Prediction and Processes. 3-5 November, 1999, New Orleans, American Meteorological Society.

Olsson, P.Q., J.Y. Harrington. 2000. Dynamics and energetics of the cloudy boundary layer in simulations of off-ice flow in the marginal ice zone. Journal of Geophysical Research (D), 105, 11889-11899.

Olsson, P.Q., K.P. Volz, H. Yi. 2003. Numerical simulations of coastal wind events in the North Gulf of Alaska. 10th Conference on Mesoscale Processes. June 23-27, Portland, Oregon (on CD-ROM)

Overland, J.E. 1984. Scale analysis of marine winds in straits and along mountainous coasts. Monthly Weather Review 112, 2530-2534.

Overland, J.E., N. Bond. 1993. The influence of coastal orography: the Yakutat storm. Monthly Weather Review 121, 1388-1397.

Overland, J.E., T.R. Hiester. 1980. Development of a synoptic climatology for the northeast Gulf of Alaska. Journal of Applied Meteorology 19, 1-14.

Pan, F., R. Smith. 1999. Gap winds and wakes: SAR observations and numerical simulations. Journal of the Atmospheric Sciences 56, 905-923.

Pielke, R.A., W.R. Cotton, R.L. Walko, C.J. Tremback, W.A. Lyons, L.D. Grasso, M.E. Nicholls, M.D. Moran, D.A. Wesley, T.J. Lee, J.H. Copeland. 1992a. A comprehensive meteorological modeling system—RAMS. Meteorology and Atmospheric Physics, 49, 69-91.

Pielke, R.A., R.L. Walko, J.L. Eastman, W.A. Lyons, R.A. Stocker, M. Uliasz, C.J. Tremback. 1992b. Recent achievements in the meteorological modeling of local weather and air quality. Trends in Atmospheric Science 1, 287-307.

Putins, P. 1966. The sequence of baric pressure patterns over Alaska. Studies on the meteorology of Alaska. First interim report, Environmental Data Service, EAAA, Washington, DC.

Reed, R.J. 1981. A case study of a bora-like windstorm in western Washington. Monthly Weather Review, 109, 2383-2393.

Reynolds, R.M., S.A. Mackli, Hiester. 1981. Observations of south Alaskan coastal winds. NOAA Tech Memo. ERL PMEL-31 Environmental Research Labs, Boulder, Co 80303 (NTIS PB82-164823.

Roebber, P.J. 1984. Statical analysis and updated climatology of explosive cyclones. Monthly Weather Review 112, 1577-1589.

Sandvik, A.D., B.R. Furevik. 2002. Case study of a coastal jet at Spitsbergen—comparison of SAR- and Model-estimated wind. Monthly Weather Review 130, 1040-1051.

Shapiro, M.A., D. Keyser. 1990: Fronts, Jet-Streams and Tropopause. In Extratropical Cyclones: the Erik Palmen Memorial Volume. C.W. Newton and E.O. Holoparnen. Eds. AMS, Boston, 167-191.

Smith R.B. 1987. Aerial observationa of the Yugoslavia bora. Journal of the Atmospheric Sciences 44 (2), 269-297.

Steenburgh, W.J., D.M. Schultz, B.A. Colle. 1998. The structure and evolution of gap outflow over the gulf of Tehuantepec, Mexio. Monthly Weather Review 126, 2673-2691.

Stevens, B.S., W.R. Cotton, G. Feingold. 1998. A critique of one-and two-dimensional models of boundary layer clouds with a binned representation of drop microphysics. Journal of Atmospheric Research 47-48, 529-533.

Stevens, B.S., W.R. Cotton, G. Feingold, C.H. Moeng. 1998. Large-eddy simulations of strongly precipitating, shallow stratocumulus-topped boundary layer. Journal of the Atmospheric Sciences 55, 3616-3638.

Uliasz, M., R.A. Stocker, R.A. Pielke. 1996. Regional modeling of air pollution transport in the southwestern United States. In Enviromental Modeling, Vol. III. P. Zannetti. Ed. Computational Mechanics Publications.

RAMS v4.3/4.4-model input namelist parameters, http://www.atmet.com/html/docs/documentation.shtml.

Whiteman, C.D. 2000. Mountain meteorology. Oxford University Press, New York.

Wallace, J.M., S. Tibaldi, A.J. Simmons. 1983. Reduction of systematic forecast errors in the ECMWF model through the introduction of an envelope orography. Quarterly Journal - Royal Meteorological Society 109 (462), 683-717.

Wallace, J.M. P. and Hobbs. 1999. Atmospheric Science—an introductory survey. Academic Press, Inc. San Diego, California.

Wilson, L.G. J.E. Overland. 1986. Meteorology of the Gulf of Alaska. In The Gulf of Alaska: Physical Environment and Biological Resources. D.W. Hood and S.T. Zimmerman. Eds. NOAA and Minerals Management Service, Anchorage, AK [MMS 86-0095, NTIS PB87-103230].

The Department of the Interior Mission

As the Nation's principal conservation agency, the Department of the Interior has responsibility for most of our nationally owned public lands and natural resources. This includes fostering sound use of our land and water resources; protecting our fish, wildlife, and biological diversity; preserving the environmental and cultural values of our national parks and historical places; and providing for the enjoyment of life through outdoor recreation. The Department assesses our energy and mineral resources and works to ensure that their development is in the best interests of all our people by encouraging stewardship and citizen participation in their care. The Department also has a major responsibility for American Indian reservation communities and for people who live in island territories under U.S. administration.

The Minerals Management Service Mission

As a bureau of the Department of the Interior, the Minerals Management Service's (MMS) primary responsibilities are to manage the mineral resources located on the Nation's Outer Continental Shelf (OCS), collect revenue from the Federal OCS and onshore Federal and Indian lands, and distribute those revenues.

Moreover, in working to meet its responsibilities, the **Offshore Minerals Management Program** administers the OCS competitive leasing program and oversees the safe and environmentally sound exploration and production of our Nation's offshore natural gas, oil and other mineral resources. The MMS **Royalty Management Program** meets its responsibilities by ensuring the efficient, timely and accurate collection and disbursement of revenue from mineral leasing and production due to Indian tribes and allottees, States and the U.S. Treasury.

The MMS strives to fulfill its responsibilities through the general guiding principals of: (1) being responsive to the public's concerns and interests by maintaining a dialogue with all potentially affected parties and (2) carrying out its programs with an emphasis on working to enhance the quality of life for all Americans by lending MMS assistance and expertise to economic development and environmental protection.